TIME AND AMPLITUDE FLUCTUATIONS OF TELESEISMIC P-SIGNALS AT NORSAR IN VIEW OF WAVE SCATTERING THEORY

A. Dahle

Royal Norwegian Council for Scientific and Industrial Research

Prepared for:

Air Force Technical Applications Center

11 July 1975

NORSAR ROYAL NORWEGIAN COUNCIL FOR SCIENTIFIC AND INDUSTRIAL RESEARCH

Scientific Report No. 4-74/75

TIME AND AMPLITUDE FLUCTUATIONS OF TELESEISMIC P-SIGNALS AT NORSAR IN VIEW OF WAVE SCATTERING THEORY

by

A. Dahle

Kjeller, July 1975

Sponsored by
Advanced Research Projects Agency
ARPA Order No. 2551

REPORT DOCUMENTATION PAGE

READ INSTRUCTIONS BEFORE COMPLETING FORM

1. REPORT NUMBER: F08606-74-C-0049	2. GOVT ACCESSION NO.
3. RECIPIENT'S CATALOG NUMBER	
4. TITLE (and Subtitle): Time and Amplitude Fluctuations of Teleseismic P-signals at NORSAR in View of Wave Scattering Theory	5. TYPE OF REPORT & PERIOD COVERED: One-time Technical
6. PERFORMING ORG. REPORT NUMBER: Scientific Report 4-74/75	
7. AUTHOR(s): A. Dahle	8. CONTRACT OR GRANT NUMBER(s): F08606-74-C-0049
9. PERFORMING ORGANIZATION NAME AND ADDRESS: NTNF/NORSAR, Post Box 51, N-2007 Kjeller, Norway	10. PROGRAM ELEMENT, PROJECT, TASK AREA & WORK UNIT NUMBERS: NORSAR Phase 3
11. CONTROLLING OFFICE NAME AND ADDRESS: VELA Seismological Center, 312 Montgomery Street, Alexandria, Va 22314	12. REPORT DATE: April 1975
	13. NUMBER OF PAGES: 83
14. MONITORING AGENCY NAME & ADDRESS (if different from Controlling Office)	15. SECURITY CLASS. (of this report)
	15a. DECLASSIFICATION/DOWNGRADING SCHEDULE

16. DISTRIBUTION STATEMENT (of this Report)

APPROVED FOR PUBLIC RELEASE, DISTRIBUTION UNLIMITED.

17. DISTRIBUTION STATEMENT (of the abstract entered in Block 20, if different from Report)

18. SUPPLEMENTARY NOTES

19. KEY WORDS (Continue on reverse side if necessary and identify by block number)

20. ABSTRACT (Continue on reverse side if necessary and identify by block number)

Theory for wave propagation in inhomogeneous media is used in a critical examination of observed P-wave travel time and amplitude anomalies. The NORSAR array data analysed exhibits several features predicted theoretically assuming the crust and upper mantle to be randomly inhomogeneous. It is demonstrated that in modelling plane wave time deviations a better fit to the observations is obtained by including a stochastical term in the plane wave equation. It is also demonstrated that wave

scattering effects is of critical importance for seismic velocity estimation when using data from small aperture arrays. In such cases, a spatial sampling of the area under investigation is recommended in order to obtain reliable velocity estimates.

AFTAC Project Authorization No.:		VT/5702/B/ETR
ARPA Order No.	:	2551
Program Code No.	:	5F10
Name of Contractor	:	Royal Norwegian Council for Scientific and Industrial Research
Effective Date of Contract	:	1 July 1974
Contract Expiration Date	:	30 June 1975
Contract No.	:	F08606-74-C-0049
Project Manager	:	Nils Marås (02) 71 69 15
Title of Work	:	Norwegian Seismic Array (NORSAR) Phase 3
Amount of Contract	:	$900 000
Contract period covered by the report	:	1 July - 30 June 1974

The views and conclusions contained in this document are those of the authors and should not be interpreted as necessarily representing the official policies, either expressed or implied, of the Advanced Research Projects Agency, the Air Force Technical Applications Center, or the U.S. Government.

This research was supported by the Advanced Research Projects Agency of the Department of Defense and was monitored by AFTAC/VSC, Patrick AFB FL 32925, under Contract No. F08606-74-C-0049.

TABLE OF CONTENTS

TABLE OF CONTENTS (Cont.)

ABSTRACT

Theory for wave propagation in inhomogeneous media is used in a critical examination of observed P-wave travel time and amplitude anomalies. The NORSAR array data analysed exhibits several features predicted theoretically assuming the crust and upper mantle to be randomly inhomogeneous. It is demonstrated that in modelling plane wave time deviations a better fit to the observations is obtained by including a stochastical term in the plane wave equation. It is also demonstrated that wave scattering effects is of critical importance for seismic velocity estimation when using data from small aperture arrays. In such cases, a spatial sampling of the area under investigation is recommended in order to obtain reliable velocity estimates.

1. INTRODUCTION

1.1 Anomalies -- Deviations from Uniform Plane Seismic Waves

Signal similarity across seismic arrays like NORSAR is an important theoretical assumption which fails to be strictly valid in practice. This report deals with the deviations from uniformity encountered at this seismological observatory, and tries to explain them by random irregularities (inhomogeneities) in the crust and upper mantle. The energy received at NORSAR seismometers from events at epicentral distances greater than 30^{o} is usually treated in terms of uniform plane waves. For n equivalent sensors comprising the array we expect the waveform to follow the mathematical formulated law:

$$A_i = A_o \qquad i = 1,\ldots,n \qquad (1.1.1)$$

$$\tau_i = \vec{r}_i \cdot \vec{u} \qquad i = 1,\ldots,n \qquad (1.1.2)$$

where A_i is the signal amplitude at the i-th sensor, A_o is the uniformly expected amplitude, τ_i is the time-shift at the i-th sensor relative to a reference time, $\vec{r}_i$ is the position vector of the i-th sensor relative to a reference point, and $\vec{u}$ is the travel time gradient (slowness).

In this report words like anomaly, deviation, residual, fluctuation and error will be used synonymously to express the imperfectness of the observed wavefield across NORSAR relative to a uniform plane wave described by eq. (1.1.1) and eq. (1.1.2). Fig. 1.1 shows a small-scale picture of the sensor configuration within subarrays 04B, 05B and 08C at NORSAR.

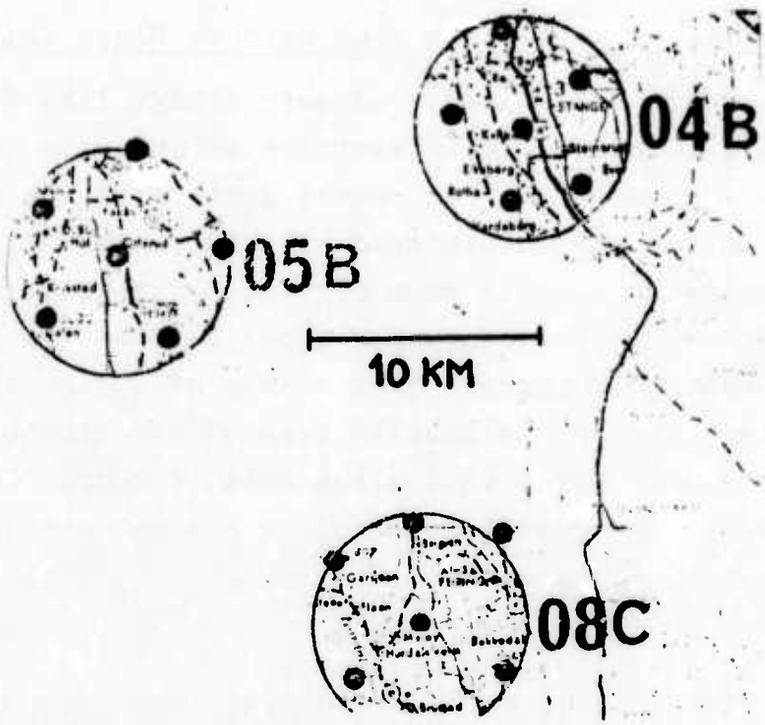

Fig. 1.1 Section showing the configuration of single sensors within NORSAR subarrays. Each black dot gives the position of a vertical short-period seismometer.

The whole array consists of 22 such subarrays (see Fig. 4.3). Fig. 1.2 illustrated what kind of deviations actually are observed at NORSAR. Delaying traces according to plane wave does not give a proper line-up. The amplitudes also show a non-uniform picture. Both these facts are in disagreement with the uniform plane wave model.

It should be stressed that the time anomalies on subarray level are physically real, not purely measurement error, and that amplitude differences are too big to be attributable to geometrical spreading or elastic attenuation.

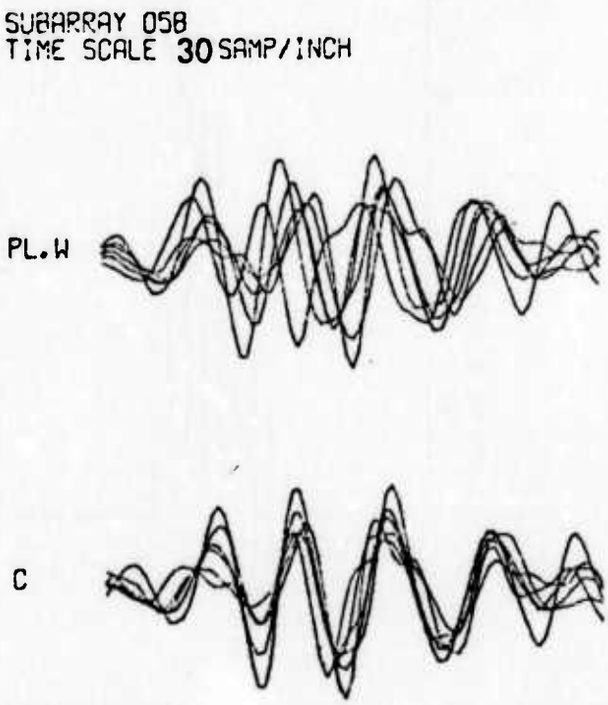

Fig. 1.2 Delayed single instrument recordings for an Aleutian event plotted in the same frame according to the best plane wave fit, denoted PL.W, and the more correct line-up determined by correlation, denoted C. Sampling rate is 20 Hz.

1.2 Travel Time Anomalies

Fig. 1.3 shows the distribution of time differences between a line-up determined by the best-fitting plane wave, and the "correct" line-up determined by correlation. The distribution seems to have a Gaussian shape. It should be noted that this distribution was obtained by considering the plane wave front deviations within subarrays and thus representative only for deviations from the plane wave shape within a small portion (7-8 km) of the wave front.

The pattern of subarray time anomalies shows no systematic trend as function of epicenter region. This is demonstrated

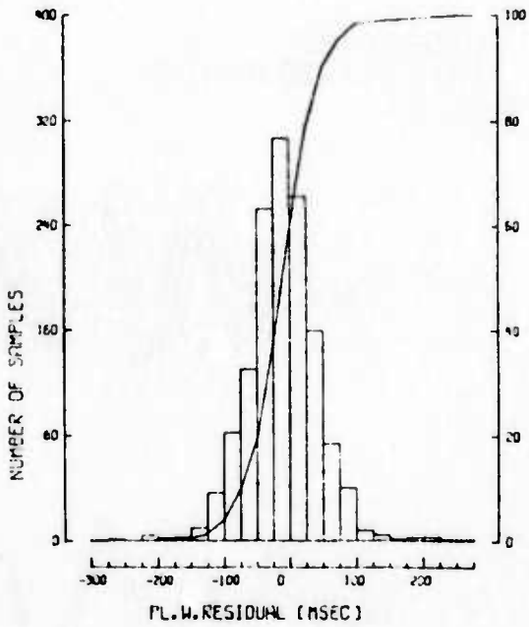

Fig. 1.3 Distribution of plane wave residuals on subarray level. The correct line-up is determined by the correlation procedure described by Gangi and Fairborn (1968). Well-recorded events filtered by a Butterworth bandpass filter in the range 0.8-2.8 Hz have been used.

by the random distribution of plane wave residuals of subarrays 05B and 12C in Fig. 1.4. On the other hand, the residuals are stationary in the sense that they repeat themselves for events from the same epicentral area. This holds even for events from regions of great structural complexity (e.g., continental margins of the Pacific Ocean) as demonstrated for subarray 03C in Fig. 1.4 The stationarity seems to indicate a near-receiver structure causing the anomalies.

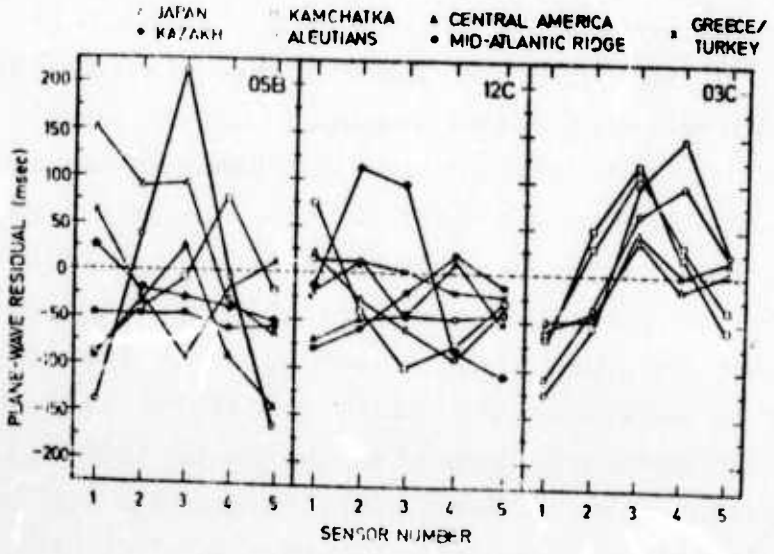

Fig. 1.4 Plane wave residuals of the type whose distribution is shown in Fig. 1.3, demonstrating the randomness (subarrays 05B and 12C) and the stationarity (subarray03C) in the pattern.

1.3 Amplitude Anomalies

The amplitude pattern across NORSAR has been subject to a statistical analysis (Husebye et al, 1974), where one of the important conclusions turns out to be the stationarity of the amplitude pattern for events from the same epicenter region. This observation agrees with the travel time observations. As for the time residuals, we are inclined to favor near-receiver structures causing this effect.

The distribution of maximum signal amplitudes across the 132 equivalent short period vertical seismometers at NORSAR is skewed to the right, i.e., higher values. Statistical tests favored a lognormal distribution, which was explained by Ringdal et al (1972) as the multiplicative effect of a multilayered earth structure. Tatarski (1961) explains a lognormal amplitude distribution in terms of wave propagation in a random medium.

1.4 The Choice of a Random Medium Model

Berteussen (1975) discusses the possibility of explaining time delay corrections at NORSAR (i.e., anomalies) by interfaces in the crust and upper mantle. He concludes that current deterministic crust and upper mantle models are able to explain only a small part of the observed anomalies. In a search for a better approach to the problem of explaining anomalies, we have found it reasonable to consider a random medium model as described theoretically by Chernov (1960). This approach has been widely used in other fields of physics, especially in acoustics and radio telemetry. The choice of a random medium model is supported by the existence of the Gaussian travel time anomaly distribution and the lognormal amplitude distribution previously mentioned.

This report will contain a condensed theoretical presentation of P-wave scattering in a randomly inhomogeneous medium. The applicability of the model for the crust and upper mantle beneath NORSAR will be discussed and compared to similar results obtained by Aki (1973) and Capon (1974) for the Large Aperture Seismic Array (LASA) in Montana, and also by Capon and Berteussen (1974) for NORSAR data. Also a refined version of the plane wave model (eq. (1.1.1) and eq. (1.1.2)) will be proposed, accounting for the stochastic part of wave field caused by random scattering.

2. THE RANDOM MEDIUM CONCEPT

2.1 Random Inhomogeneities

Deviations from homogeneity occur in every real medium. Usually observed inhomogeneities are classified in two main types, regular or random. A spatial mapping of a real stationary medium could be briefly formulated as

$$\alpha(\vec{r}) = \alpha_0 + \alpha_1(\vec{r}) + \varepsilon(\vec{r}) \qquad (2.1.1)$$

where α is some physical parameter describing the medium, α_0 is a constant, α_1 is the regularly varying term, and ε is the unknown random deviation from the deterministic part $\alpha_0 + \alpha_1(\vec{r})$. If E denotes expectation, $\varepsilon(\vec{r})$ is required to satisfy the condition

$$E\{\varepsilon(\vec{r})\} = 0 \qquad (2.1.2)$$

If regular changes in a real medium occur in some preferred direction like height in the atmosphere or depth in the earth, a useful approximation is to regard the medium as having a layered structure. Thus, if the regular term $\alpha_1(\vec{r})$ could be neglected in each layer, we could simply write for (2.1.1.)

$$\alpha(\vec{r}) = \alpha_0 + \varepsilon(\vec{r}) \qquad (2.1.3)$$

where we now have

$$E\{\alpha(\vec{r})\} = E\{\alpha_0\} + E\{\varepsilon(\vec{r})\} = \alpha_0 \qquad (2.1.4)$$

The random inhomogeneities are thus interpreted as fluctuations around the expected value of the parameter considered. Following the theory of Chernov (1960) for acoustic waves in a random medium, we shall adopt this simplified case as a starting point.

2.2 Description of a Random Medium

It should be recalled that eqs. (2.1.1) and (2.1.3) are stationary versions of time dependent forms. However, when changes in the properties of the medium are slow compared with the duration of phenomena to be studied, a time independent formulation is applicable. In the following we shall let α denote P-wave velocity, but the random medium description by the use of α will apply to the density ρ as well as the elastic parameters λ and μ.

Introducing the refractive index

$$n(\vec{r}) = \frac{\alpha_0}{\alpha(\vec{r})} \tag{2.2.1}$$

and its deviation from the mean value of unity

$$\eta(\vec{r}) = n(\vec{r}) - 1 \tag{2.2.2}$$

we describe a medium with random inhomogeneities by considering these functions as random in space. The fluctuations in wave velocity are, of course, caused by fluctuations in density and the Lamé constants.

Since in a random medium the fluctuations in the refractive index $\eta(\vec{r})$ are not known, we shall assume that its functional description represents a random process (Bendat and Piersol, 1966). The variation of the index of refraction within a volume or along a particular path is considered to be a realization or sample function from an ensemble of possible functions $\{\eta(\vec{r})\}$ ($\{\}$ denotes ensemble). The realization is considered to correspond to a point in a suitable probability space so that it is meaningful to speak about statistical or ensemble averages. Thus in order to characterize a random medium, we have to use statistical concepts where space plays the role of time in the general definition of ergodic random processes.

We shall assume that the random medium is spatially homogeneous and statistically isotropic. By spatial homogeneity we mean that whenever v is a subvolume of the random medium and $\vec{r}$ is the fixed difference between possible point locations in v with position vectors $\vec{r}'$ and $\vec{r}' + \vec{r}$ then

$$E\{N'_v(\vec{r})\} = E\{\overline{[\eta(\vec{r}')\eta(\vec{r}'+\vec{r})]_v}\} = N'(\vec{r}) \qquad (2.2.3)$$

where the bar denotes averaging over all $\vec{r}'$ within v. It is readily understood that $N'(\vec{r})$ is defined as the average product $\eta(\vec{r}')\eta(\vec{r}'+\vec{r})$ taken over the entire medium. Statistical isotropy eliminates the dependence on the direction of $\vec{r}$ so that

$$N'(\vec{r}) = N'(r) \qquad (2.2.4)$$

where r denotes the modulus of the spatial difference vector $\vec{r}$. This implies that when $|\vec{r}| = 0$

$$E\{\overline{[\eta^2]_v}\} = N'(0) \qquad (2.2.5)$$

requiring that the mean square fluctuations in the refractive index be constant throughout the random medium. In this case we define a correlation coefficient by

$$N(r) = N'(r)/N'(0) = N'(r)/\overline{\eta^2} \qquad (2.2.6)$$

As pointed out by Chernov (1960), there seems to be no simple way to determine this correlation function theoretically and a proper starting point is therefore some empirical correlation function. Experience shows that a large number of estimated correlation functions for fluctuations of physical parameters in nature approximately satisfy a correlation coefficient exponentially decreasing with distance like

$$N(r) = e^{-r/a} \qquad (2.2.7)$$

where a is constant. However, it can be shown (Chernov, 1960) that the assumption about $\eta(\vec{r})$ being a continuous function

implies that

$$\left[\frac{dN(r)}{dr}\right]_{r=0} = 0 \qquad (2.2.8)$$

The correlation function given in (2.2.7) does not satisfy this condition, and a somewhat different function satisfying (2.2.8) has to be chosen. A definition chosen by Chernov (1960) for mathematical convenience which will be assumed in the following is the Gaussian function

$$N(r) = e^{-r^2/a^2} \qquad (2.2.9)$$

where a is known as the correlation distance. This function is depicted in Fig. 2.1. The correlation distance corresponds to the point where the correlation function (2.2.9) is down to $e^{-1}=0.37$, and the statistical dependence between fluctuations

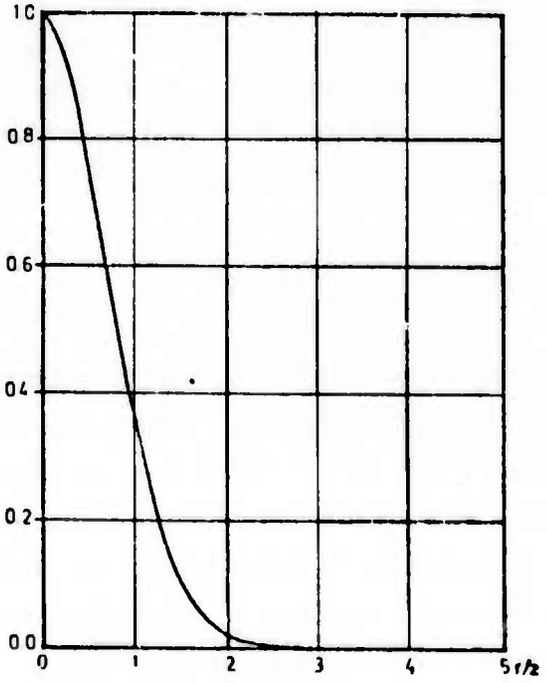

Fig. 2.1 Gaussian correlation function assumed for the refractive index fluctuations.

becomes small compared to unity. Physically the correlation distance is interpreted as the average size of the inhomogeneities in the medium, i.e., the diameter of the volume throughout which we can assume the physical conditions to be constant.

2.3 The Earth as a Random Medium

Modelling the earth, or part of it, as a random medium according to the definition in the previous two sections is a question of considerable difficulty. Due to the known variation of wave velocity with depth as well as lateral variation in this quantity, only isolated layers or volumes would perfectly pertain to the random medium concepts homogeneity and isotropy. Capon (1974) suggested to solve this problem by modelling layered structure of the earth's crust and upper mantle, with P-velocity fluctuating around a constant value within each layer. He also discusses the possibility of decomposing this model into an equivalent deterministic and an ideal random medium, where the random medium only gives rise to fluctuations in amplitude and phase. Such a model is realistic when the angles of incidence at the interfaces are small for all portions of the wave.

The earth model assumed throughout this text is the one depicted in Fig. 2.2, where random inhomogeneities are confined to the upper part of the mantle and the crust. It is obvious from this figure that the 'histories' of the two rays in the inhomogeneous medium on the source side of the path are about identical, ensuring a plane wave to enter into the inhomogeneous medium on the receiver side. This assumption is important in the application of the theory to be developed.

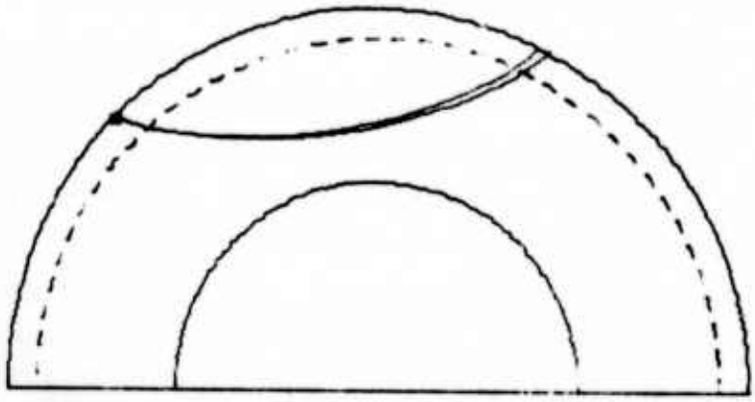

Fig. 2.2 Schematic earth model with inhomogeneities confined to the upper 500 km (beyond dotted line). The rays drawn correspond to the extreme ones for NORSAR ($\delta\Delta \approx 1$ deg).

3. SCATTERING OF P-WAVES IN A RANDOM MEDIUM

3.1 The Equation of Motion in a Weakly Inhomogeneous Medium

The only means of solution of the linear elasticity relations in an inhomogereous medium is through approximation methods which impose restrictions on the structural complexity of the medium. However, even crude approximations are justified through the practical usefulness of exact of asymptotic solutions of the wave equation. Assuming infinitesimal strain in a perfectly elastic and isotropic solid where $\vec{u}(\vec{r},t)$ denotes displacement about the equilibrium position of a point $P(\vec{r})$ we obtain from Karal and Keller (1964), applying the operator equality $\nabla^2\vec{u} = \nabla(\nabla\cdot\vec{u})-\nabla x\nabla x\vec{u}$:

$$\rho \frac{\partial^2\vec{u}}{\partial t^2} = (\lambda+2\mu)\nabla(\nabla\cdot\vec{u})+\nabla\lambda\nabla\cdot\vec{u}-\mu\nabla x\nabla x\vec{u}+\nabla\mu x(\nabla x\vec{u})+2(\nabla\mu\cdot\nabla)\vec{u} \quad (3.1.1)$$

where $\lambda(\vec{r})$, $\mu(\vec{r})$ and $\rho(\vec{r})$, the elastic moduli and density respectively, are random functions in space according to eq. (2.1.3). Theoretical seismology usually deals with wave propagation through media where gradients of the medium's characteristics are either smooth and small or abrupt. In both cases solution of eq. (3.1.1.) involves two distinct waves, dilatational and shear. The amount of coupling between these waves depends on the above-mentioned gradients (Landers, 1971).

The case to be treated here is a weakly inhomogeneous medium, where the spatial change of the elastic parameters is small as compared to the parameters themselves. In this case we simply neglect terms containing gradients of the medium's characteristics. Rewriting eq. (3.1.1) using the expression

$$\theta = \nabla\cdot\vec{u} \quad (3.1.2)$$

for dilatation, we obtain the modified form

$$\rho \frac{\partial^2\vec{u}}{\partial t^2} = (\lambda+2\mu)\nabla\theta-\mu\nabla x(\nabla x\vec{u}) \quad (3.1.3)$$

Taking the divergence of this equation, remembering that terms containing $\nabla\rho$, $\nabla\lambda$ and $\nabla\mu$ are negligible gives:

$$\rho \frac{\partial^2\theta}{\partial t^2} = (\lambda+2\mu)\nabla^2\theta \qquad (3.1.4)$$

Dividing through by $\lambda+2\mu$ we arrive at the well-known differential equation:

$$\frac{1}{\alpha^2}\frac{\partial^2\theta}{\partial t^2} - \nabla^2\theta = 0 \qquad (3.1.5)$$

where

$$\alpha = \alpha(\vec{r}) = \left[\frac{\lambda(\vec{r})+2\mu(\vec{r})}{\rho(\vec{r})}\right]^{\frac{1}{2}} \qquad (3.1.6)$$

is the velocity of the primary disturbance expressed by θ.

If the amount of variation in the elastic parameters is small, say a few per cent about the mean value, this property will certainly also be shared by the wave velocity α (cf. eq. (3.1.6)). Introducing η as defined in eq. (2.2.2) we infer that (see Chapter 2):

$$\frac{1}{\alpha^2} = \frac{n^2}{\alpha_o^2} = \frac{(1+\eta)^2}{\alpha_o^2} \qquad (3.1.7)$$

where

$$|\eta| << 1 \qquad (3.1.8)$$

The wave equation for a weakly inhomogeneous medium then finally becomes:

$$\frac{(1+\eta)^2}{\alpha_o^2}\frac{\partial^2\theta}{\partial t^2} - \nabla^2\theta = 0 \qquad (3.1.9)$$

This is the form of the wave equation for compressional elastic waves required in order to take advantage of the simplicity of Chernov's theory for acoustic waves. Note that since η is an unknown function of position, there is no easy way to solve the differential equation (3.1.9).

3.2 Rytov's Method

Random inhomogeneities cause fluctuations both in amplitude and phase. This is a statement based on practical experience (fading of radio signals, twinkling of stars) as well as theoretical considerations. Imagine a uniform plane monochromatic wave of P-type in homogeneous medium travelling into a weakly inhomogeneous medium of the type described in 2.1-2.2 (see Fig. 3.1). The primary waves in the inhomogeneous medium are assumed to satisfy eq. (3.1.9). In the homogeneous medium we write the plane wave in the standard form:

$$\theta = A_o e^{-i(\omega t - kx)} \tag{3.2.1}$$

where for simplicity the direction of the x-axis coincides with the normal to the wavefront.

Due to the effect of the inhomogeneities, eq. (3.2.1) has to be modified accordingly. The amplitude and spatial part of the phase function are now supposed to be unknown functions of position in the inhomogeneous medium, and we are looking for a solution of eq. (3.1.9) of the form:

$$\theta = A(\vec{r})\ e^{-i(\omega t - S(\vec{r}))} \tag{3.2.2}$$

The amplitude function $A(\vec{r})$ is alternatively expressed as

$$A(\vec{r}) = A_o\ e^{\log(A(\vec{r})/A_o)} \tag{3.2.3}$$

where log means the natural logarithm to be taken.

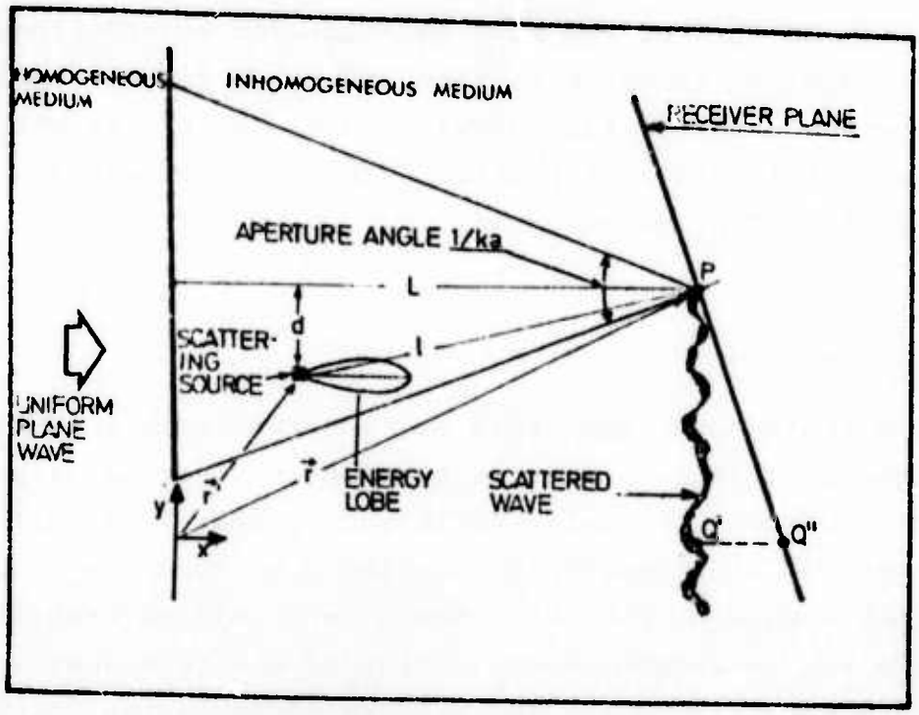

Fig. 3.1 Schematic illustration of forward scattering in an inhomogeneous medium. The scattering field at a point $P(\vec{r})$ is given as the integrated effect within a cone with vertex in P and aperture angle 1/ka (the Fresnel approximation).

Inserting this expression into eq. (3.2.2) we get

$$\theta = A_o \, e^{-i(\omega t - S(\vec{r}) + i \log(\frac{A(r)}{A_o})} = A_o \, e^{-i(\omega t - \Psi(\vec{r}))} \qquad (3.2.4)$$

where

$$\Psi(\vec{r}) = S(\vec{r}) - i \log(\frac{A(\vec{r})}{A_o}) \qquad (3.2.5)$$

The real part of the complex function Ψ is the spatial phase function $S(\vec{r})$, and the imaginary part expresses the natural logarithm of the ratio between amplitudes, $\log (A(\vec{r})/A_o)$. Note that the latter ratio also denotes the fluctuations in logarithmic amplitude (logamplitude) relative to the incident wave. The idea now is to use the right hand part of eq. (3.2.4)

in the basic wave equation for the inhomogeneous medium (eq. (3.1.9)). Doing this, we obtain an equation where θ has been replaced by Ψ, namely

$$(\nabla\Psi)^2 - i\nabla^2\Psi = (1+\eta)^2 \frac{\omega^2}{\alpha_o^2} \tag{3.2.6}$$

In the homogeneous medium the function Ψ has the form $\Psi_o = kx$ according to its definition, and satisfies the equation

$$(\nabla\Psi_o)^2 - i\nabla^2\Psi_o = k^2 \tag{3.2.7}$$

where

$$k = \frac{\omega}{\alpha_o} \tag{3.2.8}$$

is the wavenumber of the homogeneous wave.

Writing

$$\Psi = \Psi_o + \Psi_1 \tag{3.2.9}$$

we have

$$\Psi_1 = S_1 - i \log (A/A_o) \tag{3.2.10}$$

and

$$S_1 = S - kx \tag{3.2.11}$$

We are now in a position to successfully combine eq. (3.2.6) and eq. (3.2.7). Invoking eq. (3.2.9) into (3.2.6) and subtracting eq. (3.2.7) yields:

$$2\nabla\Psi_o\nabla\Psi_1 - i\nabla^2\Psi_1 = 2\eta k^2 + [\eta^2 k^2 - (\nabla\Psi_1)^2] \qquad (3.2.12)$$

The next step is to drop the terms in the square brackets under the assumption about small perturbations in the refractive index, so that η^2 can be neglected compared to η. The additional requirement is that $\frac{1}{k}\nabla\Psi_1 \sim \eta$ and according to (3.1.8) this imposes the restriction that

$$\frac{1}{k}|\nabla\Psi_1| << 1 \qquad (3.2.13)$$

Eq. (3.2.12) is then simply written as the linear differential equation.

$$2\nabla\Psi_o\nabla\Psi_1 - i\nabla^2\Psi_1 = 2\eta k^2 \qquad (3.2.14)$$

Remembering that $\Psi_o = kx$, we have

$$2k(\partial\Psi_1/\partial x) - i\nabla^2\Psi_1 = 2\eta k^2 \qquad (3.2.15)$$

and by defining a new function W related to Ψ_1 as

$$W = \Psi_1 e^{ikx} \qquad (3.2.16)$$

we obtain the inhomogeneous Helmholz equation

$$\nabla^2 W + k^2 W = i2\eta k^2 e^{ikx} \qquad (3.2.17)$$

for the function W.

3.3 Large Scale Inhomogeneities

Eq. (3.2.14) was obtained under the restriction that the phase change and relative change in amplitude per wave length is small (cf. eq. (3.2.13)). Because this essentially is a limitation on the gradient of Ψ_1, it obviously serves as a better approximation than the method of small perturbations which assumes that the perturbed quantity is small (Born approximation). However, neglecting $(\nabla\Psi_1)^2$ while retaining $\nabla^2\Psi_1$ in eq. (3.2.12) is a questionable step which has been commented on by Taylor (1967). As far as can be seen, there is no a priori reason why the two terms in the square brackets of eq. (3.2.12) simply cancel each other and thus justify an assumption of the type above.

The applicability of Rytov's method turns out to be conditioned upon the inequalities:

$$\frac{1}{k}\left|\nabla \log\left(\frac{A}{A_o}\right)\right| << 1 \qquad (3.3.1)$$

and

$$\frac{1}{k}|\nabla S_1| << 1 \qquad (3.3.2)$$

Inequality (3.3.1), which states that the scattered energy in going a wave length be small, is plausible in view of the restriction $|\eta|<<1$. Since we write

$$S = S_0 + S_1 = kx + S_1(\vec{r}) \qquad (3.3.3)$$

the inequality (3.3.2) may alternatively be written as

$$\frac{1}{k}|\nabla S| \sim 1 \qquad (3.3.4)$$

Expressing the gradient of S as components in a rectangular coordinate system (see Fig. 3.1), we have

$$\left|\frac{\partial S}{\partial x}\right| \sim k, \qquad \left|\frac{\partial S}{\partial y}\right| << k, \qquad \left|\frac{\partial S}{\partial z}\right| << k \tag{3.3.5}$$

These expressions show that the transverse components of the gradient of the phase (i.e., the transverse wave wavenumber components) are small compared to the longitudinal component. This means that the direction of propagation for waves in the inhomogeneous medium deviates only slightly from the original direction in the homogeneous medium.

Sharply directed scattering is known to be produced by large scale inhomogeneities where the condition

$$ka >> 1 \tag{3.3.6}$$

is fulfilled (Morse and Feshbach, 1953). In inhomogeneous media of this type we can neglect back-scattering and wave reflection in the sense that the energy lobe for a point source on the wave front will have the form illustrated in Fig. 3.1. This serves as a simplification for the solution of eq. (3.2.17) at a point $P(\vec{r})$ in the inhomogeneous medium. The actual solution of eq. (3.2.17) is a Green's function problem (Morse and Feshbach, 1953) and the general form is:

$$W = -\frac{1}{4\pi}\int_V \frac{i2\eta k^2}{\ell} e^{i(k(\ell+x'))}\, dv \tag{3.3.7}$$

where $\ell = |\vec{r}-\vec{r}'|$ in accordance with the symbols used in Fig. 3.1. V is the part of the inhomogeneous medium contributing significantly to the solution at the point P. The assumptions about large scale inhomogeneities justify the limitation of the volume V to the layer which lies between the base of the inhomogeneous medium (x=0 in Fig. 3.1) and P, and within a cone with its vertex at P and an aperture angle of the order 1.0/ka (see Fig. 3.1).

Within these limits we approximate the length

$$\ell = ((x-x')^2 + d^2)^{\frac{1}{2}} \tag{3.3.8}$$

by

$$\ell \sim x-x' + \frac{1}{2}\frac{d^2}{x-x'} \tag{3.3.9}$$

where

$$d^2 = (y-y')^2 + (z-z')^2 \tag{3.3.10}$$

Multiplying eq. (3.3.7) by e^{-ikx} we obtain the solution for the function Ψ_1 yielding:

$$\Psi_1 = -\frac{ik^2}{2\pi} \int_V \frac{\eta}{\ell} e^{ik(\ell-(x-x'))}\, dv \tag{3.3.11}$$

Replacing $1.0/\ell$ by $1.0/x-x'$ and substituting in the exponent of eq. (3.3.11) from eq. (3.3.9) gives

$$\Psi_1 = -\frac{ik^2}{2\pi} \int_V \frac{\eta}{x-x'} e^{ik\left(\frac{d^2}{2(x-x')}\right)}\, dv \tag{3.3.12}$$

Taking real and imaginary parts, we finally obtain the expressions for the scattered field:

$$S_1 = \frac{k^2}{2\pi} \int_0^x \int_{-\infty}^{+\infty} \int_{-\infty}^{\infty} \frac{\sin(kd^2/2(x-x'))}{x-x'} \eta(x',y',z')dx'dy'dz' \tag{3.3.13a}$$

$$\log A/A_o = \frac{k^2}{2\pi} \int_0^x \int_{-\infty}^{+\infty} \int_{-\infty}^{\infty} \frac{\cos(kd^2/2(x-x'))}{x-x'} \eta(x',y',z') \, dx'dy'dz' \tag{3.3.13b}$$

These equations, which turn out to correspond to the Fresnel approximation in diffraction theory (Jenkins and White, 1957), are the starting point for the statistical derivations. Noteworthy, eqs. (3.3.13) may be thought of as the analytical expressions for the effects causing crinkled wavefronts to P-waves. In the next chapter these effects will be implemented in a refined model for travel time and logamplitude observations.

3.4 Statistical Quantities of the Scattered Wave Field

Since a detailed derivation of the statistical aspects of the wave scattering problem has been carried out by Chernov (1960), only main formulae will be summarized and important steps stressed in this section.

Assuming that the receiver, i.e., our seismograph, is located at the point Q' with spatial cartesian coordinates (L,0,0) (cf. Fig. 3.1), our first aim is to obtain expressions to the mean square fluctuations in phase and logamplitude. Using the symbol Φ for the phase fluctuations S_1, and Λ for the logamplitude fluctuations $\log(A/A_o)$, we rewrite eqs. (3.3.13a,b) as:

$$\Phi = \int_0^L \int_{-\infty}^{+\infty} \int F_1(L-x',k,d)\eta(x',y',z')dx'dy'dz' \qquad (3.4.1a)$$

$$\Lambda = \int_0^L \int_{-\infty}^{+\infty} \int F_2(L-x',k,d)\eta(x',y',z')dx'dy'dz' \qquad (3.4.1b)$$

where F_1 and F_2 are easily deduced from eq. (3.3.13a,b). Squaring each of these expressions and taking the average, remembering from section 2.2 that

$$\overline{\eta(\vec{r}')\eta(\vec{r}'')} = N'(|\vec{r}'-\vec{r}''|) = \overline{\eta^2}N(r) \qquad (3.4.2)$$

where

$$r^2 = (x'-x'')^2 + (y'-y'')^2 + (z'-z'')^2 \qquad (3.4.3)$$

we have

$$\overline{\Phi^2} = \overline{\eta^2} \int_0^L \int_0^L \int_{-\infty}^{+\infty} \int F_1(L-x',k,d')F_1(L-x'',k,d'')N(r) \qquad (3.4.4a)$$

$$dx'dy'dz'dx''dy''dz''$$

$$\overline{\Lambda^2} = \overline{\eta^2} \int_0^L \int_0^L \int_{-\infty}^{+\infty} F_2(L-x',k,d')F_2(L-x'',k,d'')N(r) \quad (3.4.4b)$$

$$dx'dy'dz'dx''dy''dz''$$

Using linear coordinate transformations and variable shifts, we obtain under the assumption of

$$L >> a \quad (3.4.5)$$

that

$$\overline{\Phi^2} = \frac{\sqrt{\pi}}{2} \overline{\eta^2}\, k^2\, a\, L \left(1 + \frac{1}{D} \arctan D\right) \quad (3.4.6a)$$

$$\overline{\Lambda^2} = \frac{\sqrt{\pi}}{2} \overline{\eta^2}\, k^2\, a\, L \left(1 - \frac{1}{D} \arctan D\right) \quad (3.4.6b)$$

provided

$$D = \frac{4L}{ka^2} \quad (3.4.7)$$

a dimensionless quantity denoted wave parameter, is intermediate or large compared to unity. Note that the case $D<<1$ is excluded. An important result is that the ratio RMS (root mean square) logamplitude to RMS phase given by

$$\frac{\sigma\Lambda}{\sigma\Phi} = \left(\frac{\overline{\Lambda^2}}{\overline{\Phi^2}}\right)^{\frac{1}{2}} = \left[\frac{1 - \frac{1}{D} \arctan D}{1 + \frac{1}{D} \arctan D}\right]^{\frac{1}{2}} \quad (3.4.8)$$

is a quantity always less than unity.

A more complete characterization of the statistical properties of the wave field is achieved by using correlation functions. The cross correlation between logamplitude and phase fluctuations analogous to (3.4.4) is given by:

$$\overline{\Phi\Lambda} = \eta^2 \int_0^L \int_0^L \int_{-\infty}^{+\infty} F_1(L-x',k,d')F_2(L-x'',k,d'')N(r) \quad (3.4.9)$$

$$dx'dy'dz'dx''dy''dz''$$

Applying linear transformations and variable shifts and assuming as before $L>>a$, eq. (3.4.9) yields for D intermediate or large compared to one:

$$\overline{\Phi\Lambda} = \frac{\sqrt{\pi}}{16} \eta^2 k^2 a^3 \log (1+D^2) \quad (3.4.10)$$

We are now able to find an expression for the correlation coefficient of the logarithmic amplitude and phase fluctuations at a point Q'(L,0,0). Using for this quantity the definition:

$$r_{\Phi\Lambda} = \frac{\overline{\Phi\Lambda}}{\sqrt{\Phi^2}\sqrt{\Lambda^2}} \quad (3.4.11)$$

we have

$$r_{\Phi\Lambda} = \frac{1}{2} \frac{\log (1+D)^2}{\sqrt{D^2-(\arctan D)^2}} \quad (3.4.12)$$

Note that if we consider D as a measure for the linear extent of the inhomogeneous medium, the correlation which exists at small distances vanishes as D grows since $r_{\Phi\Lambda}$ approaches log D/D.

The next step is to consider the question of autocorrelation of phase (or logamplitude) at different receiving points. Assume that our receivers are located along the direction of propagation. Let the coordinates of the receivers be (L,0,0) and (L+ΔL,0,0) corresponding to Q' and Q'' in Fig. 3.1. The longitudinal autocorrelation for the phase fluctuations are given by:

$$R_\Phi(\Delta L) = \overline{\eta^2} \int_0^L \int_0^{L+\Delta L} \int_{-\infty}^{+\infty} F_1(L-x',k,d')F_1(L+\Delta L-x'',k,d'')$$

$$N(r)dx'dx''dy'dy''dz'dz'' \qquad (3.4.13)$$

It should be noted that because of the directional character of the scattered energy, waves scattered in the layer bounded by the planes x=L and x=L+ΔL are incident on the second but not on the first receiver. Therefore these waves can be neglected in calculating the autocorrelation replacing the limits corresponding to the integration variable dx' by L instead of L+ΔL. Variable shifts, linear tranformations of origin and the condition L>>a justify the formula

$$r_\Phi(\Delta L) = R_\Lambda(\Delta L) = \frac{\frac{\sqrt{\pi}}{2}\,\overline{\eta^2}\,k^2 a\,L}{1 + (\frac{2\Delta L}{ka^2})^2} \qquad (3.4.14)$$

where $R_\Lambda(\Delta L)$ is the longitudinal autocorrelation for log-amplitude fluctuations defined as eq. (3.4.13) with F_1 replaced by F_2. Eq. (3.4.14) was obtained under the assumption that D is large compared to unity.

For large values of D we can write eqs. (3.4.6) in the form

$$\overline{\Phi^2} = \overline{\Lambda^2} = \frac{\sqrt{\pi}}{2}\,\overline{\eta^2}k^2 a\,L \qquad (3.4.15)$$

Defining the correlation coefficients

$$r_\Phi(\Delta L) = \frac{R_\Phi(\Delta L)}{\overline{\Phi^2}}, \quad r_\Lambda(\Delta L) = \frac{R_\Lambda(\Delta L)}{\overline{\Lambda^2}} \qquad (3.4.16)$$

we have

$$r_\Phi(\Delta L) = r_\Lambda(\Delta L) = \frac{1}{1 + (\frac{2\Delta L}{ka^2})^2} \qquad (3.4.17)$$

This formula shows that if ΔL~a, then the fluctuations in the longitudinal direction are almost completely correlated in a large scale weakly inhomogeneous medium (ka>>1). Defining the longitudinal correlation distance as the distance

ΔL_k where the correlation coefficient is down to 0.5, we have

$$\Delta L_k = \frac{ka^2}{2} \tag{3.4.18}$$

Eq. (3.4.17) corresponds to a correlation function quite commonly used for representing the anomalous gravity field of the earth (Heiskanen and Moritz, 1967).

Finally we look at the expressions for the transverse autocorrelation of the amplitude and phase fluctuations. We shall let the receivers be located tangentially to the wave front like P and Q' with coordinates (L,y,0) and (L,0,0) respectively. Expressions for the fluctuations are still given by eqs. (3.4.1) replacing d by $d' = \sqrt{(y-y')^2+z'^2}$ for receiver P and $d'' = \sqrt{y''^2+z''^2}$ for receiver Q'.

The transverse autocorrelation for phase fluctuations is given by:

$$R_\Phi(y) = \overline{\eta}^2 \int_0^L \int_0^L \int_{-\infty}^{+\infty} F_1(L-x',k,d')F_1(L-x',k,d'')N(r) \tag{3.4.19}$$

$$dx'dx''dy'dy''dz'dz''$$

$R_\Lambda(y)$, the transverse autocorrelation for logamplitude, is analogously given by eq. (3.4.19) replacing F_1 by F_2.

Defining normalized functions as before

$$r_\Phi(y) = \frac{R_\Phi(y)}{\overline{\Phi}^2}, \qquad r_\Lambda(y) = \frac{R_\Lambda(y)}{\overline{\Lambda}^2} \tag{3.4.20}$$

Chernov has shown to obtain for L>>a and large values of D the formulae:

$$r_{\phi}(y) = \frac{e^{-y^2/a^2} - \frac{1}{D}\{\frac{\pi}{2} - Si(\frac{y^2}{Da^2})\}}{1 - \frac{1}{D}\arctan D} \qquad (3.4.21a)$$

$$r_{\Lambda}(y) = \frac{e^{-y^2/a^2} + \frac{1}{D}\{\frac{\pi}{2} - Si(\frac{y^2}{Da^2})\}}{1 + \frac{1}{D}\arctan D} \qquad (3.4.21b)$$

where

$$Si(x) = \int_0^x \frac{\sin t}{t}\, dt \qquad (3.4.22)$$

The graphs of the functions (3.4.21a,b) with D=10 are shown in Fig. 3.2 compared to the correlation functions for the fluctuations in the refractive index. Note that because of

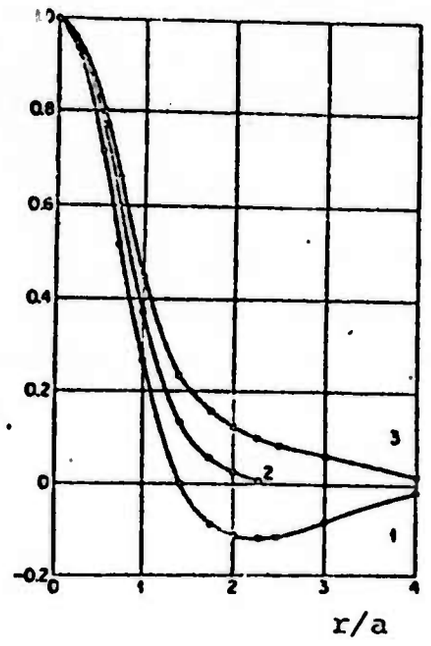

Fig. 3.2 Transverse autocorrelation function for phase (3) and logamplitude (1) together with the Gaussian correlation function (2). Redrawn from Chernov (1960).

the rotational symmetry assumed, y should be interpreted as the distance r between receivers tangentially to the wave front rather than the coordinate in a specified direction.

The important result to stress is that the transverse autocorrelation functions for logamplitude and phase extend to a distance of the order of the correlation distance in the medium. Recently, Christoffersson (1974) has pointed out that eqs. (3.4.21) are valid for $y/a \lesssim 1$ since Chernov did the approximation

$$e^{\left(-\left(\frac{y^2}{a^2}\,\frac{1}{ka}\right)^2\right)} \sim 1 \qquad (3.4.23)$$

to obtain these equations. Christoffersson (1975) suggests using a series expansion in the actual approximations to obtain transverse autocorrelation functions valid for a wide range of y/a and D values. In this work no attempt has been made to correct eqs. (3.4.21) for y/a values considerably larger than 1, and this should be remembered below.

3.5 Classification by the Wave Parameter D

Seismological wave propagation problems fall into three main categories depending on the wave parameter

$$D = \frac{4L}{ka^2} = \frac{2}{\pi} \cdot \frac{L}{a} \cdot \frac{\lambda}{a} \qquad (3.5.1)$$

Limiting the discussion to the case $ka \gg 1$, i.e., large scale inhomogeneities, we have:

1) The region $D \ll 1$ where the Uniform Plane Wave Model can be used. As the extent L increases and approaches the correlation distance in size, we have to account for the variation in the physical properties.

2) When $D \tilde{<} 1$, Ray-Theory might be applicable.

3) The region $D \tilde{>} 1$ where Diffraction-Theory is necessary and the stochastic behavior of the wave field should be regarded as significant.

The preceding theory treats P and S as uncoupled waves, where P energy is converted into P energy due to the inhomogeneities in the medium. Knopoff and Hudson (1964, 1967) show that P→S and S→P conversion can safely be neglected compared to P→P under circumstances when $ka >> 1$. The important thing to remember is that deviations from the weakly inhomogeneous case certainly exist in the real earth, and that these deviations may lead to considerable P→S conversion as well as back-scattering effects.

Point (3) in the previous classification scheme requires a statistical attitude to seismic problems. An important assertion put forward and made use of in the following is the normality in the distribution of the random variables Φ and Λ. In fact, if the entire distance L which contributes to the values of Φ and Λ is divided into segments of the order of the correlation distance, then the changes in Φ and Λ along different segments will be almost statistically independent. According to the Central Limit Theorem of probability theory, when the number of independent segments is large, quantities like Φ and Λ will obey the normal distribution law.

4. THE APPLICABILITY OF CHERNOV'S MODEL

4.1 Selection of Data

Normally, frequency domain analysis of data is preferred when formulae obtained involve the wavenumber k as in Chapter 3. On the other hand, using spectra calculated from a data window according to some estimated or assumed slowness introduces at least two error sources. First of all, back-scattering or coda effects at the end of the window is likely to play a role. Secondly, the estimate of window start time is associated with some bias or measurement error. Time domain analysis was therefore regarded as favorable in this case. Narrow bandpass filtering was obtained by exposing the 20 Hz sampled signals to a Butterworth 3rd order lowpass filter followed by a similar highpass filter. The combined filter shows a very distinct peak response at the average frequency and was advantageous compared to conventional narrow bandpass filters with a reasonable number of bandpass coefficients. For analysis purposes 10 teleseismic P events were chosen as the basic data source. Other selection criteria were good signal-to-noise ratio as well as coverage in azimuth and velocity. NOAA epicenter information for all events is given in Table 1.

It was decided to measure travel time and amplitude as soon as possible after the onset of each event, thereby eliminating as much as possible of the back-scattering and coupling effects. From a computer-plotted display of the filtered traces the peak (or trough) of the first (or second) cycle was uniformly identified by visual inspection. At the same time sensors with bad performance due to communication problems were masked in order to avoid abnormal data in the computer programs. The exact travel time and amplitude for the identified phase were determined as the extremum of a parabola fitted to seven points around the peak. The accuracies in these time and amplitude determinations are not easily figured out since the exact value of what we are trying to measure is unknown.

Event No.	NOAA EPICENTER INFORMATION				Region
	Date (m/d/y)	Origin Time (h m s)	Vel (km/s)	Azi (deg)	
1 (*)	11/21/72	17.01.55.3	17.27	11.42	Aleutians
2 (*) (***)	12/10/72	03.35.48.2	17.91	36.51	Japan
3 (*)	05/17/73	09.38.09.9	14.9	81.31	Kazakh
4 (*) (***)	08/06/72	01.12.50.4	14.61	113.06	Iran
5 (*) (**)	04/18/72	15.07.49.1	17.04	160.25	Tanganyika
6 (*) (***)	04/11/72	02.21.15.7	17.35	223.36	Mid-Atlantic
7 (*)	07/27/71	02.02.49.6	23.95	267.15	Peru
8 (*)	07/09/72	12.10.54.7	22.13	293.17	Mexico
9 (*)	07/08/71	14.00.00.1	18.80	318.10	Nevada
10 (*) (**)	03/26/71	17.35.18.0	15.75	343.78	Alaska

TABLE 1

Events used in analysis

(*) Events filtered at 0.7 Hz used in estimating Chernov (1960) parameters and in slowness estimation problems

(***) Events filtered also at 0.9, 1.1 and 1.3 Hz.

See references to these symbols in the text.

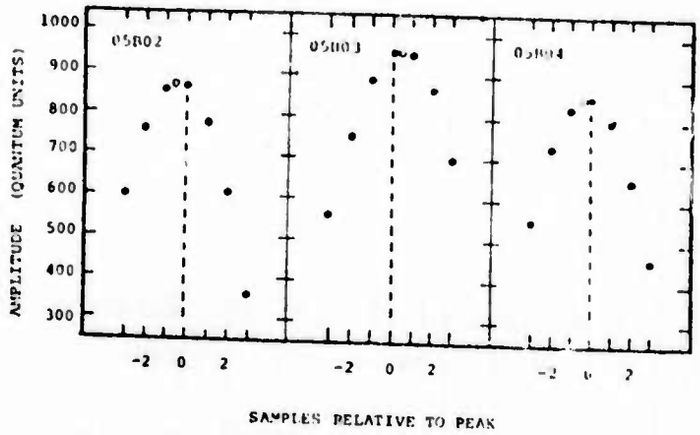

Fig. 4.1 Determination of exact travel time and amplitude (open circle) by fitting a parabola to seven points around the peak sample (black dots). Sampling interval is 0.05 sec.

A few examples of determination of peaks by this method are shown in Fig. 4.1, from which we conclude that the measured times are certain within a fraction of a sampling interval of 50 milliseconds. Of course, this conclusion is based on an assumption about sufficient coherency in the signals. All the observed times were reduced to common observation plane by correcting for differences in altitude among the seismic stations. This correction was done using the apparent velocity determined by the NORSAR Event Processor (EP) Gjøystdal (1973). Finally, it should be mentioned that the EP determined velocity and azimuth were always used when projecting horizontal distances between sensors into the wave front to obtain the transversal distance (PQ' as opposed to PQ'' in Fig. 3.1).

4.2 Modelling the Anomalies in Multidimensional Seismic Observations

The validity of the principles outlined in this chapter will be quite general, although the headline tries to relate the content to a special topic, namely, seismic measurements. Since the data analysis in the following will be carried out for a network or an array of stations, there will be a need for multidimensional concepts in terms of vectors and matrices. In this specific context T will denote a column vector of n observations. The quantity expressed by T will be either phase travel times or logamplitudes as observed by n different sensors for short periodic compressional waves. The expected value of the vector T is the vector of expectations of its elements (Morrison, 1967). If E denotes expectation, we have

$$E\{T\} = \begin{bmatrix} E\{t_1\} \\ \vdots \\ E\{t_n\} \end{bmatrix} \qquad (4.2.1)$$

where $t_1,\ldots,t_n$ are the individual elements of T.

The concept expectation is extended to represent any linear model formulation in an appropriate coordinate system. This means that we may write

$$E\{T\} = RU \qquad (4.2.2)$$

where R is an n x p matrix of coordinates and U is a p x 1 vector of p appropriate regression coefficients. For simplicity we do not distinguish explicitly between matrices and vectors.

An illustration of the applicability is given in Fig. 4.2, where the observed travel time (or logamplitude) field across an array of seismic stations is schematically decomposed into a linear deterministic trend effect superposed by a spatially

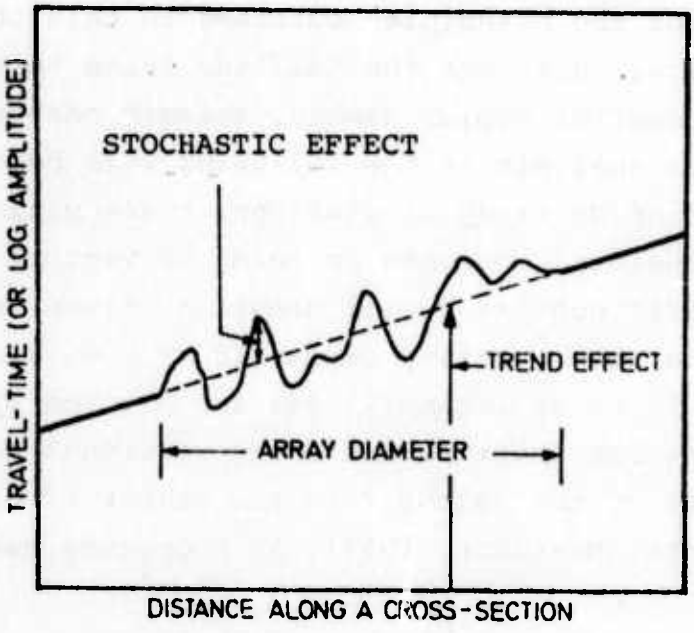

Fig. 4.2 Schematic illustration of a linear deterministic trend model superposed by a stochastic scattering effect.

stochastic effect S assumed to satisfy:

$$E\{S\} = 0 \tag{4.2.3}$$

S may be thought of as a vector of n elements analog to T in eq. (4.1.1).

The idea here is that the effects depicted in Fig. 4.2 are the dominating components in the observed compressional wavefield. S corresponds to the stochastic fluctuations given by eqs. (3.3.13), and which are physically interpreted as the scattering response of an inhomogeneous crust and upper mantle. Note that no measurement error or noise effect has been included in Fig. 4.1, as these terms are thought of as only producing small ripples on the solid line representing the total field.

If the location of seismic sensors is expressible in a local two-dimensional cartesian coordinate system with x and y axes pointing W→E and S→N respectively, then the deterministic effect in the travel time field is readily expressed in terms of slowness-components (U_x, U_y) (Gjøystdal, 1973). An improved model for the observed times is then given according to:

$$t_i = \begin{bmatrix} 1 \\ r_{ix} \\ r_{iy} \end{bmatrix} \cdot \begin{bmatrix} t_o \\ U_x \\ U_y \end{bmatrix} + s_i + \varepsilon_i \qquad i=1,2,\ldots,n \qquad (4.2.4)$$

where (r_{ix}, r_{iy}) are the position vector components for the i-th station, s_i is random scattering effect and ε_i is measurement error or noise. According to eq. (4.2.1) we have from eq. (4.2.2) that

$$E\{t_i\} = E\{t_o + r_{ix}U_x + r_{iy}U_y + s_i + \varepsilon\}$$

$$= t_o + r_{ix}U_x + r_{iy}U_y \qquad i=1,\ldots,n \qquad (4.2.5)$$

since

$$E\{s_i\} = E\{\varepsilon_i\} = 0 \qquad (4.2.6)$$

When t_i represents logamplitude, U_x and U_y are logamplitude gradients in the x,y-plane. No such gradients are observed in real data and we may set

$$U_x = U_y = 0 \qquad (4.2.7)$$

This is also reasonable in view of magnitude correction tables which allow for maximum 5 per cent variation in amplitude within a 1 degree teleseismic distance interval, corresponding to the diameter of NORSAR. For logamplitudes we then write

the model

$$\log A_i = \log A_o + a_i + e_i \qquad i=1,\ldots,n \tag{4.2.8a}$$

where a_i is the scattering terms and e_i measurement error for logamplitude. Thus we have

$$E\{\log A_i\} = \log A_o \tag{4.2.8b}$$

If we let $t_o = \log A_o$, $s_i = a_i$, $\varepsilon_i = e_i$, we see that eq. (4.2.4) may represent time and logamplitude simultaneously, of course, with obvious modifications.

In matrix formulation eq. (4.2.4) is written

$$T = TU + S + \epsilon$$

where

$$\left.\begin{aligned} T = \begin{bmatrix} t_1 \\ \vdots \\ t_n \end{bmatrix} \qquad R = \begin{bmatrix} 1 & r_{1x} & r_{1y} \\ \vdots & \vdots & \vdots \\ 1 & r_{nx} & r_{ny} \end{bmatrix} \\ U = \begin{bmatrix} t_o \\ U_x \\ U_y \end{bmatrix} \qquad S = \begin{bmatrix} s_1 \\ \vdots \\ s_n \end{bmatrix} \qquad \epsilon = \begin{bmatrix} \varepsilon_1 \\ \vdots \\ \varepsilon_n \end{bmatrix} \\ i=1,\ldots,n \end{aligned}\right\} \tag{4.2.9}$$

At this stage it is natural to introduce the extended variance notation for the n component vector T, defined as

$$E\{(T-E\{T\})(T-E\{T\})^*\} = E\{(T-RU)(T-RU)^*\} = E\{SS^*\} = \quad (4.2.10)$$

$$= \begin{bmatrix} \sigma_{11}^2 & \sigma_{12}^2 \cdots & \sigma_{1n}^2 \\ \sigma_{21}^2 & \sigma_{22}^2 & \sigma^2 \\ \vdots & \vdots & \\ \sigma_{n1}^2 & & \sigma_{nn}^2 \end{bmatrix} = \Sigma$$

$$\sigma_{ij}^2 = E\{(t_i-E\{t_i\})(t_i-E\{t_i\})^*\} , \quad i,j=1,\ldots,n.$$

* (star) denotes transponation and ϵ is for convenience included in the S term.

The normalized version of eq. (4.2.10) is obtained dividing each element σ_{ij}^2 by $\sigma_{ii}\sigma_{jj}$ yielding the correlation matrix

$$C = \begin{bmatrix} 1 & C_{12} \cdots & C_{1n} \\ C_{21} & 1 \quad \cdots & \\ \vdots & & \vdots \\ C_{n1} \cdots & & 1 \end{bmatrix} \quad (4.2.11)$$

The matrix C is invariant under changes of scale and origin of the variates in T.

Considering an array of relatively closely space seismometers at the earth's surface to be located approximately transversally to the wave front, then the correlation coefficient C_{ij} of eq. (4.1.11) is given by eqs. (3.4.21) provided Chernov's (1960) theory for wave scattering is considered to be acceptable. The existence of matrices Σ and C significantly different from a diagonal and identity matrix respectively means that there is in general an all-to-all dependence between our observations. More precisely formulated: the anomaly (fluctuation) at a particular point depends on its neighboring points in space both in size and sign. The conventional simple linear least squares method neglects this interaction, modelling (4.2.9) as:

$$T = RU + \epsilon' \qquad (4.2.12)$$

where $\epsilon' = S + \epsilon$ is considered simply as an error residue vector.

4.3 Estimation of the Anomaly Covariance Matrix

The covariance matrix Σ or the correlation matrix C is the quantity which has to be evaluated in order to check the validity of the theoretical predictions of Chapter 3. However, there are two difficult problems here which will be discussed in some detail in the following. One is tied to the estimate of the reference value $\hat{U}$ used when calculating the anomalies. If the "true" value is U, then $\hat{U} = U + \delta U$ where δU is an error which we do not know. We have:

$$E\{(T-R\hat{U})(T-R\hat{U})^*\} = E\{(T-R(U+\delta U)(T-R(U+\delta U))^*\} = \qquad (4.3.1)$$

$$= E\{(S-S\delta U)(S-R\delta U)^*\} = E\{SS^*\} + E\{(R\delta U)(R\delta U)^*\}$$

Cross-terms $E\{S(R\delta U)^*\} = E\{(R\delta U)S^*\} = 0$, because S is a random vector. The contribution from the error covariance matrix $E\{(R\delta U)(R\delta U)^*\}$ in estimating Σ (eq. 4.2.10) depend on δU as well as the coordinate matrix R, i.e., the fixed array configuration. Large R may result in a considerable error even if the elements in δU are small.

There are considerable difficulties associated with the evaluation of statistical quantities using a fixed array like NORSAR. Since the medium under consideration, the upper portion of the real earth, is considered random in space and not in time, we meet severe sampling problems. Events separated in time but not in space will produce the same response to the inhomogeneities, i.e., the same anomalies will be observed within the limits of measurement error and difference due to frequency content and energy release. With events separated in

space there is still a considerable overlap in "sampling" the inhomogeneities. By "sampling" overlap or redundancy sampling is meant that different signals pass through part of the same structures such that observations are not statistically independent. Statistical independence in turn is ruled by the correlation distance of the random medium. A mobile array would be able to overcome most of these sampling problems.

In order to estimate the covariance matrix Σ, 10 events with optimum coverage in azimuth and velocity were selected. As rotational symmetry of the covariance matrix Σ is assumed, the effect of using the events with approach to NORSAR as depicted in Fig. 4.3 would be to reduce the effect of strong local structures not pertaining to the randomly inhomogeneous medium. Each event produces a sample matrix of Σ and the

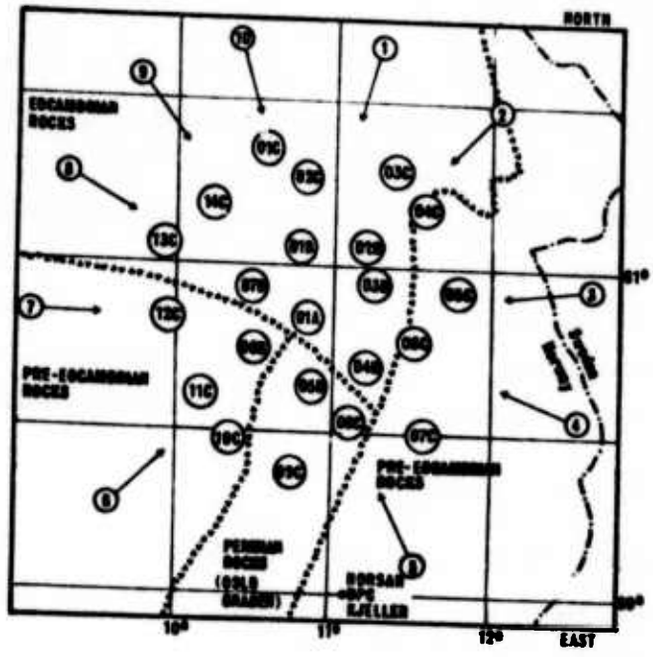

Fig. 4.3 Direction of approach to NORSAR for events used in estimating the empirical correlation functions, events 1-10 in Table 1.

average of 10 sample matrices yielded an estimate $\hat{\Sigma}$. All traces were filtered in order to pass through the energy at 0.7 Hz.

In view of the estimation problems discussed previously, it was decided to base the reference $\hat{U}$ on the slowness determined from the NOAA epicenter solution. For logamplitudes the best reference was considered to be the statistical mean of all available sensors. The transformation of $\hat{\Sigma}$ to $\hat{C}$ (Section 4.2) needs a few comments. Based on theoretical considerations, one would expect that the variances of $\hat{\Sigma}$ to be homogeneous. This was not in fact true, and we can think of at least three possible explanations

1) Too few samples
2) A redundancy sampling effect
3) Local structure effects.

Note that 1) and 2) are in a certain sense inversely related to each other since increasing the number of events to obtain better estimates results in a more severe redundancy sampling effect. However, the averaging procedure in going from the 132 x 132 element matrix $\hat{C}$ to the associated correlation function is of course a means to improve estimates and avoid redundancy sampling, since different portions of the whole array represent approximately independent samples of the medium.

The correlation functions were constructed by simply averaging over elements in $\hat{C}$ corresponding to station separations within each [(0.5-N)km, (0.5+N)km], N=1,2,...,100 interval. The Fisher Z-transformation (Cramér, 1945) for the correlation values was avoided due to the obvious uncertainty in the data. The obtained correlation functions are depicted in Figs. 4.4a,b, together with the theoretical Chernov (1960) functions (3.4.6a,b).

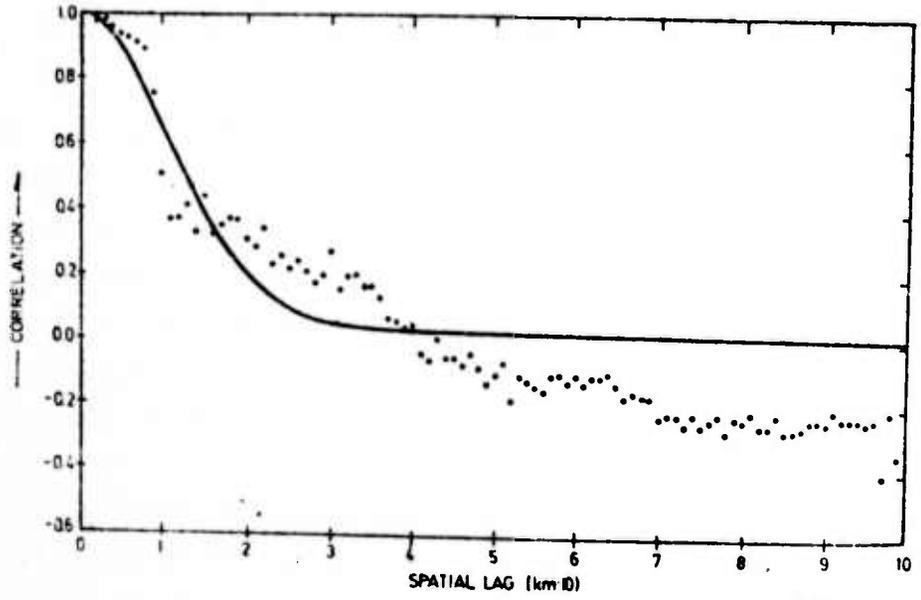

(a)

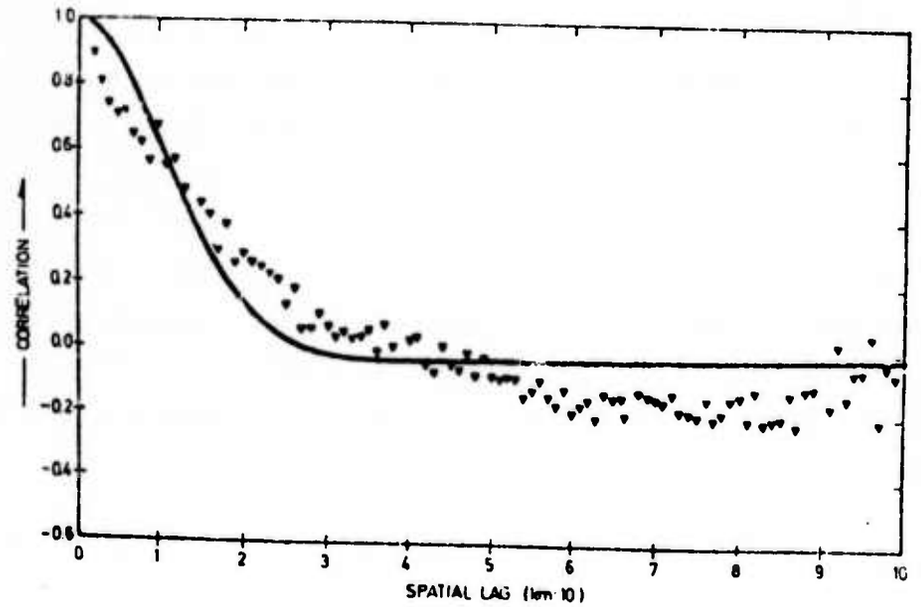

(b)

Fig. 4.4 Empirical transverse correlation functions for travel time fluctuations (a) and logamplitude fluctuations (b) together with the theoretical Chernov (1960) functions eqs. (3.4.21a,b) with correlation distance 15 km and wave parameter 10.

4.4 Comparison of Observations with Chernov's Theoretical Predictions

The wave parameter D can be determined either by eq. (3.4.8) from an estimate of $\sigma\Lambda/\sigma\Phi$ or by using eq. (3.4.12) and an estimate of the correlation coefficient between phase and logamplitude. These two determinations are independent and offer, as point out by Aki (1973) a severe test on the applicability of Chernov's theory to observed values. Consequently, the quantities $\sigma\Lambda$, $\sigma\Phi$ and $r_{\Phi\Lambda}$ were estimated for events 1-10 in Table 1 at 0.7 Hz and for events 2, 4 and 6 at 0.9, 1.1 and 1.3 Hz. $\sigma\Lambda$ was computed referred to the mean logamplitude and $\sigma\Phi$ relative to the best fitting plane wave. Φ is defined as $\Phi = \Delta t \cdot \omega$ where ω is angular frequency and Δt is the plane wave residual. Results are presented in Table 4. Note that the number of sensors used is seldom 132 due to array operating discrepancies.

Following Aki's procedure to plot the results in $\sigma\Lambda/\sigma\Phi$ versus $r_{\Phi\Lambda}$ diagram, they are easily compared to the theoretical predicted relationship obtained by eliminating D from eq. (3.4.8) and eq. (3.4.12). Fig. 4.5 shows how the NORSAR data fit into the picture presented by Aki for LASA data using a somewhat different measurement procedure. Capon's (1974) average result based on 273 measurements, represented by a big black dot, is also shown. The lower part of Fig. 4.5 gives the average of events 2, 4 and 6 in Table 1 for different frequencies.

Confidence limits for the two estimators $\hat{r}_{\Phi\Lambda}$ and $\sigma\hat{\Lambda}$ $\sigma\hat{\Phi}$ have to be considered before any conclusions can be reached. Introducing the Fisher Z-transformation (Cramér, 1945) to the correlation coefficient $r_{\Phi\Lambda}$, it is shown that the variable Z defined as

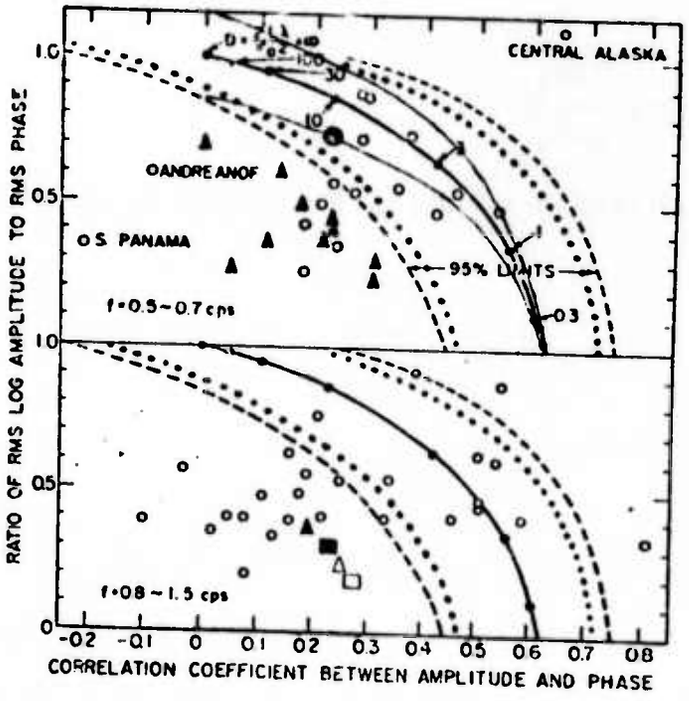

Fig. 4.5 $\sigma\Lambda/\sigma\Phi$ versus $r_{\Phi\Lambda}$ diagrams redrawn from Aki (1973). All text pertains to his original figure.

Symbol definition

Upper box:

- Chernov's theoretical relationship
- 95% confidence limits for Aki's (1973) observations (66 samples)
- Aki's (1973) observations for LASA
- Confidence limits for $r_{\Phi\Lambda}$ estimates in this study based on 111 samples
- Confidence limits for $\sigma\Lambda/\sigma\Phi$ estimates in this study based on 111 samples
- ▲ Estimates for events 1-10 (0.7 Hz) in Table 4
- ● Capon's (1974) average reported value for LASA at 0.8 Hz (sample size 279)

Lower box:

- ▲ Average of events 2, 4 and 6 at 0.7 Hz
- ■ Average of events 2, 4 and 6 at 0.9 Hz
- △ Average of events 2, 4 and 6 at 1.1 Hz
- □ Average of events 2, 4 and 6 at 1.3 Hz.

$$Z = \frac{1}{2} \log \frac{1+\hat{r}_{\Phi\Lambda}}{1-\hat{r}_{\Phi\Lambda}} \tag{4.4.1}$$

may be considered a normally distributed variable with mean:

$$\bar{Z} = \frac{1}{2} \log \frac{1+r_{\Phi\Lambda}}{1-r_{\Phi\Lambda}} + \frac{r_{\Phi\Lambda}}{2(N-1)} \tag{4.4.2}$$

and standard deviation

$$\sigma_Z = \frac{1.0}{\sqrt{N-3}} \tag{4.4.3}$$

where N is the number of samples used in the correlation coefficient estimate.

The inverse transformation of (4.4.1) yields

$$\hat{r}_{\Phi\Lambda} = \tan h\ (Z) \tag{4.4.4}$$

and the confidence limits for $\hat{r}_{\Phi\Lambda}$ are obtained by first computing the limits for Z and then using eq. (4.4.4) to obtain the limits for $\hat{r}_{\Phi\Lambda}$. The 95% confidence limits for Z are $\bar{Z} \pm 2\sigma_Z$ and the limits for $\hat{r}_{\Phi\Lambda}$ are

$$\begin{aligned} r_{\Phi\Lambda 1} &= \tan h(\bar{Z}-2\sigma_Z) \\ r_{\Phi\Lambda 2} &= \tan h(\bar{Z}+2\sigma_Z) \end{aligned} \tag{4.4.5}$$

where $r_{\Phi\Lambda 1}$ and $r_{\Phi\Lambda 2}$ denote the lower and upper 95% confidence limits for $\hat{r}_{\Phi\Lambda}$ respectively.

The average cross correlation coefficient $\hat{r}_{\Phi\Lambda}$ estimated for event 1-10 at 0.7 Hz is 0.18 for a sample size of N=1240. Assume now that our H_0 hypothesis is

$$H_0 : r_{\Phi\Lambda} = 0 \tag{4.4.6}$$

The confidence limits for $\hat{r}_{\Phi\Lambda}$ are given by (4.4.5) to be

$$r_{\Phi\Lambda 1} = -0.06 \text{ and } r_{\Phi\Lambda 2} = 0.06$$

Thus the probability of doing an error when rejecting the hypothesis (4.4.6) is less than 5% provided the measurement based on 1240 samples lies outside the range (-0.06,0.06). The measured value of $r_{\Phi\Lambda}$ was 0.18 and is indeed very significant. The transverse cross correlation function for logamplitude and phase fluctuations was not developed by Chernov (1960). However, by calculating the best plane wave phase anomalies and the logamplitude anomalies relative to the statistical mean value, an empirical estimate $\hat{\Sigma}_{\Phi\Lambda}$ was produced. Assuming as before rotational symmetry, we obtained the cross correlation function depicted in Fig. 4.6.

The confidence limits for the ratio $\hat{\sigma}\Lambda/\hat{\sigma}\Phi$ are also interesting to know. Suppose Λ and Φ are independent and normally distributed $N(O,\sigma_\Lambda)$ and $N(O,\sigma_\Phi)$ respectively. The quantitites Λ and Φ' where

$$\Phi' = \frac{\sigma\Lambda}{\sigma\Phi} \cdot \Phi \tag{4.4.7}$$

are still independent and normally distributed. The variance ratio

$$f^2 = \frac{\hat{\sigma}^2_\Lambda}{\hat{\sigma}^2_{\Phi'}} \tag{4.4.8}$$

is known to be F-distributed (Cramér, 1945), and since

$$\sigma_{\Phi'} = \sigma_\Phi \cdot \frac{\sigma_\Lambda}{\sigma_\Phi} = \sigma_\Lambda \tag{4.4.9}$$

we obtain

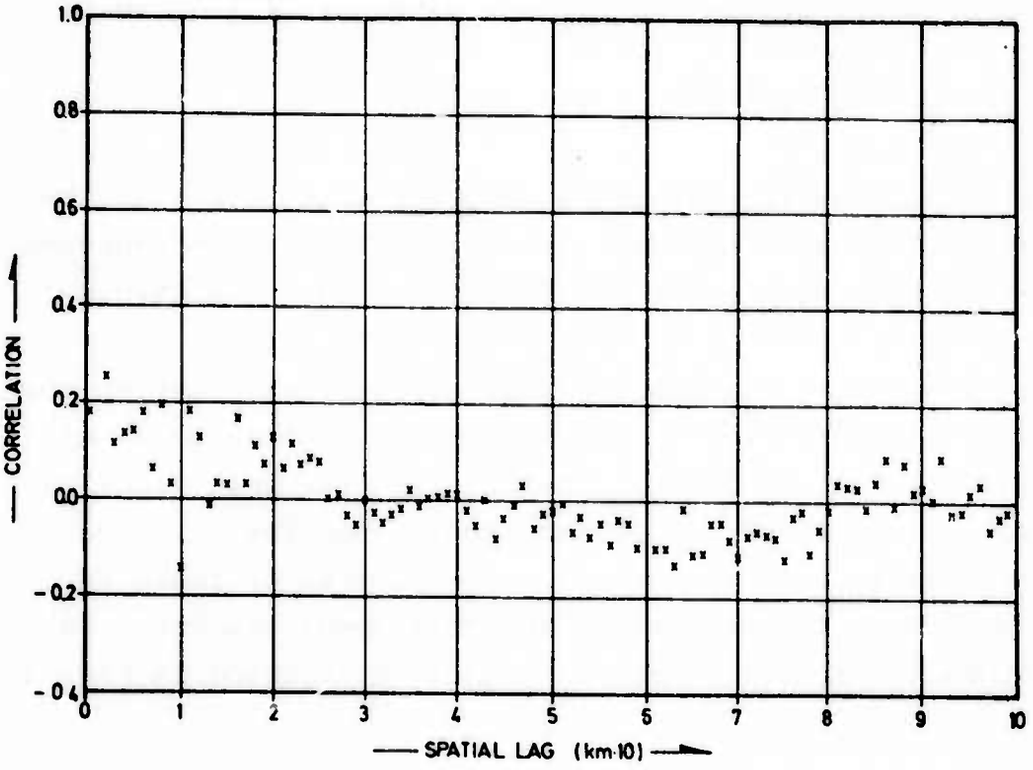

Fig. 4.6 Empirical transverse cross-correlation between phase and logamplitude fluctuations at NORSAR.

$$f^2 = -\frac{\hat{\sigma}^2_{\Lambda}\ \sigma^2_{\Lambda}}{\hat{\sigma}^2_{\Phi}\ \sigma^2_{\Phi}} \tag{4.4.10}$$

If the 95% confidence limits for f^2 are denoted γ_1^2 and γ_2^2 respectively, we have

$$\gamma_1^2 \leq f^2 \leq \gamma_2^2 \tag{4.4.11}$$

which, using (4.4.10), leads to

$$\frac{\sigma_\Lambda}{\sigma_\Phi}\,\gamma_1 \leq \frac{\hat{\sigma}_\Lambda}{\hat{\sigma}_\Phi} \leq \frac{\sigma_\Lambda}{\sigma_\Phi}\,\gamma_2 \qquad (4.4.12)$$

From an F-distribution table we find that for estimates with $N_\Lambda = N_\Phi = 111$ degrees of freedom (cf. Table 4), we have $\gamma_1 = 0.85$ and $\gamma_2 = 1.17$. The confidence intervals for estimates of the ratio $\sigma_\Lambda/\sigma_\Phi$ is then within the curves determined by

$$0.85\,\frac{\sigma_\Lambda}{\sigma_\Phi} \leq \frac{\hat{\sigma}_\Lambda}{\hat{\sigma}_\Phi} \leq 1.17\,\frac{\sigma_\Lambda}{\sigma_\Phi} \qquad (4.4.13)$$

These curves are drawn as thin solid lines in Fig. 4.5 and show that except for very large values of D ($\sigma_\Lambda/\sigma_\Phi$ very close to unity) they lie entirely inside the confidence limits for the correlation coefficient $r_{\Phi\Lambda}$.

As inferred from Fig. 4.5, all NORSAR points are outside the confidence region for Chernov's (1960) theoretical predictions. In order to see what effect the independently determined NOAA slowness estimates (cf. Table 1) have on the results depicted in Fig. 4.5, the relevant calculations of $\hat{\sigma}_\Lambda/\hat{\sigma}_\Phi$ and $\hat{r}_{\Phi\Lambda}$ were performed using these values. Results are shown in the upper part of Fig. 4.7. Also the NOAA slowness corrected for a dipping Moho with updip 94 deg from North, dip 6 deg and velocity contrast 6.6/8.2 was used as reference for the $\hat{\sigma}_\Phi$ calculations. This particular interface was shown by Berteussen (1975) to explain maximum of the NORSAR time corrections. Results using this reference are shown in the lower part of Fig. 4.7. As can be seen, both alternatives increase the σ_Φ estimate and scatter the data.

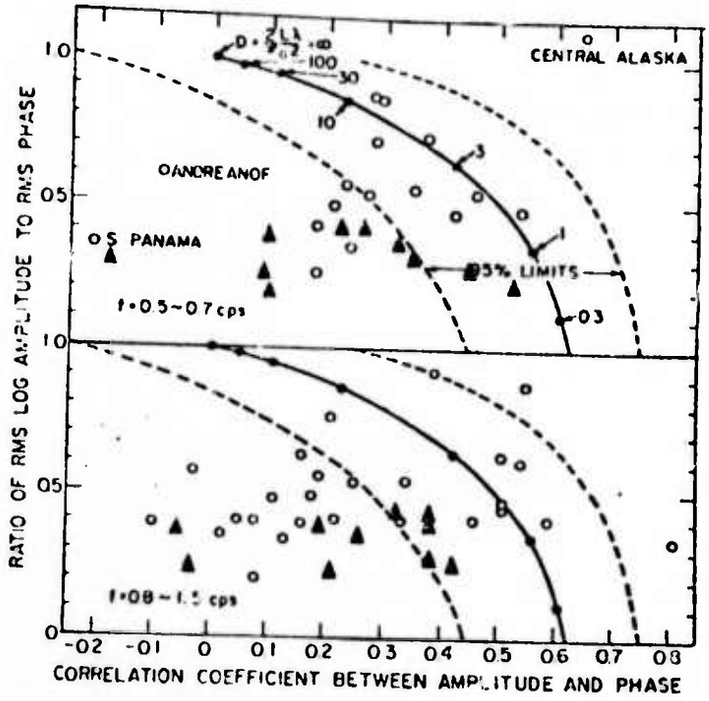

Fig. 4.7 See symbol definition of Fig. 4.5.

Upper box:

The symbols Δ give σ_A/σ_Φ versus $r_{\Phi A}$ estimates obtained for events 1-10 (Table 1) at 0.7 Hz using slowness estimated from NOAA epicenter solution and a symmetrical earth model with standard velocity distribution.

Lower box:

Same as in upper box, but with slowness corrected for dipping Moho with updip 6 deg in direction 94 deg from North and a velocity contrast of 6.6/8.2.

Normality in the distribution of travel time (phase) fluctuations is one of the important features of a wave field scattered in an isotropic inhomogeneous medium. Fig. 4.8 shows a histogram of plane wave residuals formed by the data from which σ_Φ estimates of Fig. 4.5 are constructed. It is quite clear that we are concerned with a skewed distribution which may lead to an over-estimation of σ_Φ values. Berteussen (1974) also obtained this distribution with other data.

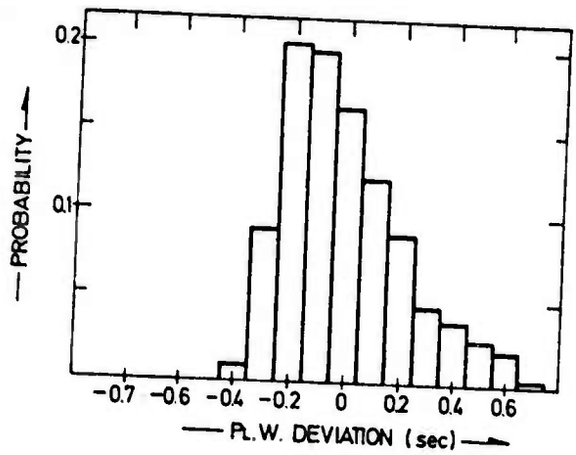

Fig. 4.8 Distribution of best plane wave deviations for events 1-10, Table 1.

The interesting question is whether this skewness has a geophysical explanation. Local high velocity bodies within the crust are likely to produce deviations of this type. In our opinion, such potential bodies of high velocity give too strong scattering locally underneath NORSAR, thus violating the conditions of the Chernov (1960) medium and shifting the $\sigma_\Lambda/\sigma_\Phi$ estimates of Fig. 4.5 below the confidence limits. Anyway, the hypothesis about random scattering taking place according to a Chernov (1960) type of medium has to be rejected on the basis of the test provided by the $\sigma_\Lambda/\sigma_\Phi$ versus $r_{\Phi\Lambda}$ computations in this study.

The previously referred studies for LASA data by Aki (1973) and Capon (1974) both give estimates for the parameters $\bar{\eta}^2$, a and L characterizing a Chernov (1960) type of crust and upper mantle. Aki (1973) limits his estimation to those data which fell inside the confidence regions (dashed lines) in Fig. 4.5. Capon (1974) used a marginal average value to compute his

parameters. Capon and Berteussen (1974) using NORSAR data obtained zero correlation between amplitude and phase fluctuations and decided that the scattering beneath NORSAR was too strong for the Chernov type of medium to be valid in the frequency range 0.6 to 2.0 Hz. As mentioned previously, these works were based on spectral data and somewhat different measurement procedures. Recently Berteussen et al (1975) estimated Chernov (1960) parameters from the data prepared for this study, using the method described by Christoffersson (1975). However, this method does not include the $\sigma_\Lambda/\sigma_\Phi$ versus $r_{\Phi\Lambda}$ test on the applicability of Chernov's theory, and is rather based on the hypothesis that Chernov's theory is valid. The hypothesis could not be rejected from the parameter values obtained.

The phase fluctuations beneath NORSAR are obviously too strong to accept that the crust and upper mantle beneath NORSAR act like a Chernov medium. On the other hand, the "abnormal" phase fluctuations do not seem to violate the predicted positive cross correlation $r_{\Phi\Lambda}$. As inferred from Table 2 $\hat{r}_{\Phi\Lambda} = 0.18$ in average for event 1-10 in Table 1, which is a reasonable value. Assuming an uncertainty of about one kilometer, we read from Fig. 4.4 that the correlation distance is about 15 km. With a mean velocity α_0=8 km/sec in the crust and upper mantle, corresponding to k=0.55 rad/km at 0.7 Hz, we are able to determine the depth L from the definition of D (eq. 3.4.7). As we can see, the Fresnel-approximation of ka being much larger than 1.0 is supported by a value:

$$ka \simeq 8.2$$

From eq. (3.4.12), we obtain:

$$D = 15 >> 1$$

Event No.	Freq. (Hz)	$\sigma\Lambda$	$\sigma\Phi$ (rad)	$\sigma\Lambda/\sigma\Phi$ (rad^{-1})	$r_{\Phi\Lambda}$	Number of samples
1	0.7	0.48	1.06	0.45	0.23	123
2	0.7	0.56	1.15	0.49	0.19	111
3	0.7	0.39	0.93	0.42	0.23	131
4	0.7	0.33	1.22	0.27	0.31	124
5	0.7	0.42	0.70	0.60	0.15	131
6	0.7	0.34	0.95	0.36	0.12	120
7	0.7	0.33	1.08	0.30	0.31	131
8	0.7	0.40	1.00	0.40	0.22	119
9	0.7	0.43	0.61	0.70	0.00	118
10	0.7	0.31	1.09	0.28	0.06	132
Aver-age	0.7	0.40	0.98	0.41	0.18	1240
2	0.9	0.57	1.44	0.40	0.25	111
4	0.9	0.38	1.55	0.25	0.29	124
6	0.9	0.37	1.20	0.31	0.16	120
2	1.1	0.59	1.77	0.33	0.30	111
4	1.1	0.42	1.90	0.22	0.31	124
6	1.1	0.40	1.48	0.27	0.14	120
2	1.3	0.69	2.10	0.29	0.34	111
4	1.3	0.44	2.26	0.19	0.32	124
6	1.3	0.43	1.75	0.24	0.12	120

TABLE 2

Root mean square fluctuations in phase Φ and logamplitude Λ are given together with the correlation between these fluctuations $r_{\Phi\Lambda}$. Number of samples corresponds to number of sensor recordings available for a particular event.

The depth of the inhomogeneous medium is then fixed to

$$L \simeq 464 \text{ km} \geq a \simeq 15 \text{ km}$$

The mean square fluctuations $\bar{\eta}^2$ of the refractive index can be determined either from an estimate of $\bar{\Lambda}^2$ and eq. (3.4.6.b) or $\bar{\Phi}^2$ and eq. (3.4.6.a).

The former quantity gives (see Table 2)

$$\bar{\eta}^2 = 0.000095 \ll 1 \tag{4.4.12}$$

The Born-approximation is valid for small fractional energy losses $\Delta I/I$ where:

$$\Delta I/I = \sqrt{\pi}\, \bar{\eta}^2\, k^2 a\, L(1-e^{-k^2a^2}) \tag{4.4.13}$$

Computing this quantity using logamplitude fluctuation yields

$$\Delta I/I = 0.35 \tag{4.4.14}$$

which is on the edge of an acceptable value. On the other hand, using phase fluctuations for determining the refractive index fluctuations we get:

$$\bar{\eta}^2 = 0.00046 \tag{4.4.15}$$

and

$$\Delta I/I = 1.74 \tag{4.4.16}$$

Conclusively, we infer that the theoretical formulae lead to a contradiction when phase information are used in the estimation of refractive index fluctuations and fractional energy loss (cf. eq. (4.4.16)). If we consider the less restrictive Rytov-approximation done to obtain the formulae in Chapter 3, requiring that the energy lost per wave length be small, we

obtain values satisfying our assumptions. Finally, we observe from the lower part of Fig. 4.5 that increasing frequency is likely to correspond to lower values of D in agreement with the formula:

$$D = 4L/ka^2 = \frac{2}{\pi}\frac{L\lambda}{a^2} \qquad (\lambda \text{ denotes wave length}) \qquad (4.4.17)$$

On the other hand, the applicability of the Chernov theory is not improved for higher frequencies.

5. THE STOCHASTIC TERM IN THE REFINED MODEL FOR TIME AND LOGAMPLITUDE

5.1 Generalized Least Squares Estimation and Prediction

The transverse autocorrelation functions shown in Figs. 4.4a,b give striking evidence for the stochastic term introduced in paragraph 4.2. Conventional modelling according to the simple least squares model represented by eq. (4.2.12) presupposes:

$$E\{\epsilon'\} = 0 \tag{5.1.1}$$

$$E\{\epsilon'\epsilon'^*\} = \sigma_\epsilon^2 \cdot I \tag{5.1.2}$$

(I is the identity matrix), and the essential constraint is

$$\text{minimum} \left(\sum_{i=1}^{n} \epsilon_i^2 \right) \tag{5.1.3}$$

The problem with correlated residuals can be circumvented by linear-transforming observations using the covariance matrix $\Sigma = E\{SS^*\}$. Disregarding abnormal cases, Σ is a positive definite matrix. Then it is invertible and expressible as (Ferguson, 1967)

$$\Sigma = XX \tag{5.1.4}$$

where X is also a positive definite invertible n x n matrix.

Including the negligible error term ϵ' in the S-term and transforming our variables through X^{-1} yields for eq. (4.2.9):

$$X^{-1}T = X^{-1}RU + X^{-1}S \tag{5.1.5}$$

Now, since

$$E\{(X^{-1}T-E\{X^{-1}T\})\ (X^{-1}T-E\{X^{-1}T\})^*\} = E\{(X^{-1}S)(X^{-1}S)^*\}$$

$$X^{-1}E\{SS^*\}X^{-1} = X^{-1}\Sigma X^{-1} = X^{-1}XXX^{-1} = I \qquad (5.1.6)$$

our observations have been transformed into uncorrelated data with qualifications satisfying eq. (5.1.1) and 5.1.2). The simple least squares technique can now be applied to the variables requiring that we perform minimization of:

$$(X^{-1}S)^*(X^{-1}S) = S^*\Sigma^{-1}S \qquad (5.1.7)$$

The covariance or correlation matrices of our data provide information which can be taken advantage of in order to predict values at certain points in space. At this stage it is convenient to introduce the combined procedure of generalized least squares estimation and prediction as actually done in Dahle et al (1975). Assume coefficients for the linear trend have to be estimated from n basic observations, and that the observed field is to be predicted at m other points. Including as before the measurement error term ϵ' in the stochastic term S, we obtain, using matrix designations and the concept of partitioned matrices:

$$T = RU + BS \qquad (5.1.8)$$

where

$$T = \begin{bmatrix} t_1 \\ \vdots \\ t_n \end{bmatrix} \qquad (5.1.9)$$

$$R = \begin{bmatrix} 1 & r_{1x} & r_{1y} \\ \vdots & & \\ 1 & r_{nx} & r_{ny} \end{bmatrix} \qquad (5.1.10)$$

$$U = \begin{bmatrix} t_o \\ U_x \\ U_y \end{bmatrix} \tag{5.1.11}$$

$$B = [I_{nn}, O_{nm}] = n \text{ rows} \left\{ \begin{bmatrix} 1 & 0 & \cdots & 0 & 0 & \cdots & 0 \\ 0 & 1 & & & \cdot & & \cdot \\ \vdots & & & & & & \\ 0 & & & 0 & 0 & \cdots & 0 \end{bmatrix} \right. \tag{5.1.12}$$

$$\underbrace{\qquad}_{n \text{ columns}} \qquad \underbrace{\qquad}_{m \text{ columns}}$$

$$S = \begin{bmatrix} S_n \\ S_m \end{bmatrix} = \begin{bmatrix} s_1 \\ \vdots \\ s_n \\ s_{n+1} \\ \vdots \\ s_{n+m} \end{bmatrix} \tag{5.1.13}$$

And provided that the covariances matrix

$$\Sigma = E\{SS^*\} = \begin{bmatrix} \Sigma_{nn} & \Sigma_{nm} \\ \Sigma_{mn} & \Sigma_{mm} \end{bmatrix} \tag{5.1.14}$$

is known, the estimates $\hat{0}$ and $\hat{S}$ are given by:

$$\hat{0} = M^{-1}R^*N^{-1}T \tag{5.1.15}$$

$$\hat{S} = \Sigma B^*N^{-1}(T-R\hat{0}) \tag{5.1.16}$$

where

$$N = B\Sigma B^* \tag{5.1.17}$$

$$M = R^*N^{-1}R \tag{5.1.18}$$

Then we obtain

$$N = [I_{nn}, O_{nm}] \begin{bmatrix} \Sigma_{nn} & \Sigma_{nm} \\ \Sigma_{mn} & \Sigma_{mm} \end{bmatrix} \begin{bmatrix} I_{nn} \\ O_{nm} \end{bmatrix} = \Sigma_{nn} \qquad (5.1.19)$$

$$\Sigma B^* = \begin{bmatrix} \Sigma_{nn} & \Sigma_{nm} \\ \Sigma_{mn} & \Sigma_{mm} \end{bmatrix} \begin{bmatrix} I_{nn} \\ O_{nm} \end{bmatrix} = \begin{bmatrix} \Sigma_{nn} \\ \Sigma_{mn} \end{bmatrix} \qquad (5.1.20)$$

We have:

$$\hat{U} = (R^*\Sigma_{nn}^{-1}R)^{-1} R^*\Sigma_{nn}^{-1}T \qquad (5.1.21)$$

which is the generalized least squares formula for estimating the linear trend in the n basic observation points (Johnston, 1963). We also see that

$$\hat{S} = \begin{bmatrix} \hat{S}_n \\ \hat{S}_m \end{bmatrix} = \begin{bmatrix} \Sigma_{nn} \\ \Sigma_{mn} \end{bmatrix} \Sigma_{nn}^{-1} (T-R\hat{U}) \qquad (5.1.22)$$

This gives

$$\hat{S}_n = T-R\hat{U} \qquad (5.1.23)$$

as we would have expected, and

$$\hat{S}_m = \Sigma_{mn}\Sigma_{nn}^{-1} (T-R\hat{U}) \qquad (5.1.24)$$

which is the prediction formula for the m points to be predicted.

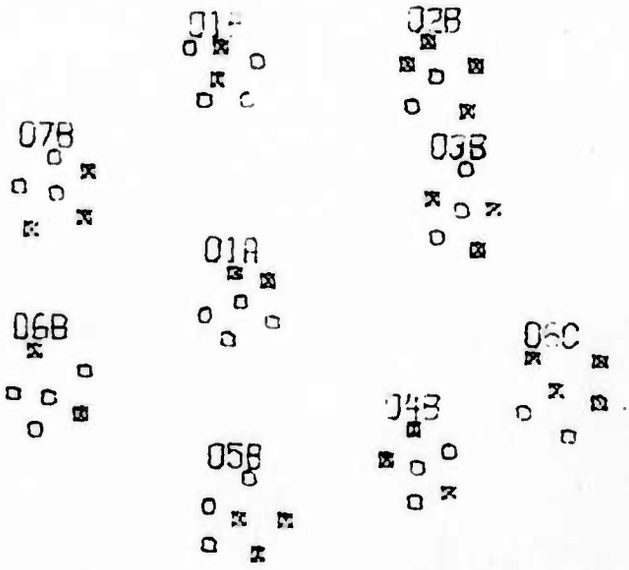

Fig. 5.1 Basic points (crossed) and points to be predicted (open).

The general all-to-all dependence which exists in the travel time and amplitude fluctuations of a network of stations like NORSAR deserves considerable attention. The estimation and prediction theory for dependent variables provides a convenient tool to study the significance of correlated data, being stochastic fluctuations or not. The special procedure undertaken was to randomly select half of the 54 stations comprising subarrays 01A, 01B-07B and 06C as basic observation points, trying to predict the observed values at the remaining ones by estimating eq. (5.1.21) and eq. (5.1.24). Basic points are marked with crosses in Fig. 5.1, while the open symbols are points where travel time (or logamplitude) has to be predicted. The quantity used as a goodness of fit

of the data to the stochastic model represented by eq. (4.2.9) is sum of squared differences between observed and predicted values, a quantity we shall prefer to denote prediction error variance.

In order to obtain a meaningful comparison, the same quantity using the simple least squared determined plane wave solution is computed. This is nothing else than the conventional sum of squared plane wave residuals when we speak of travel time. The ratio of the prediction error variances in per cent is a measure of the applicability of the stochastic model, in such a way that a hundred per cent means no improvement relative to simple least squares, while zero per cent means complete agreement with the stochastic model.

As inferred from Chapter 3, practical application of eq. (5.1.21) and (5.1.23) involves implementation of the matrix Σ or its related matrix C. The latter is easily obtained from eqs. (3.4.21a,b) or alternatively from the empirical correlation functions.

Since the Chernov functions depend essentially on correlation distance and the wave parameter D, an iterative computer program was constructed in order to determine the pair (a,D) which gives the minimum prediction error variance. Due to the very time-consuming matrix inversions involved it was considered unrealistic to try to obtain a minimum prediction error variance based on some convergence criterion. Instead, after some tentative runs on the computer, it was decided to construct a grid of points (a,D) for reasonable values of these quantities and compute the relative prediction error variance for these points. The distance between grid points was chosen as 3 km for correlation distance and 10 for wave parameter. Based on the calculated grid, a contour plot was drawn on the computer by linear interpolation contouring the lines of constant relative prediction error variance. Results for three events are shown in Fig. 5.2a,b,c,d,e,f for different frequencies.

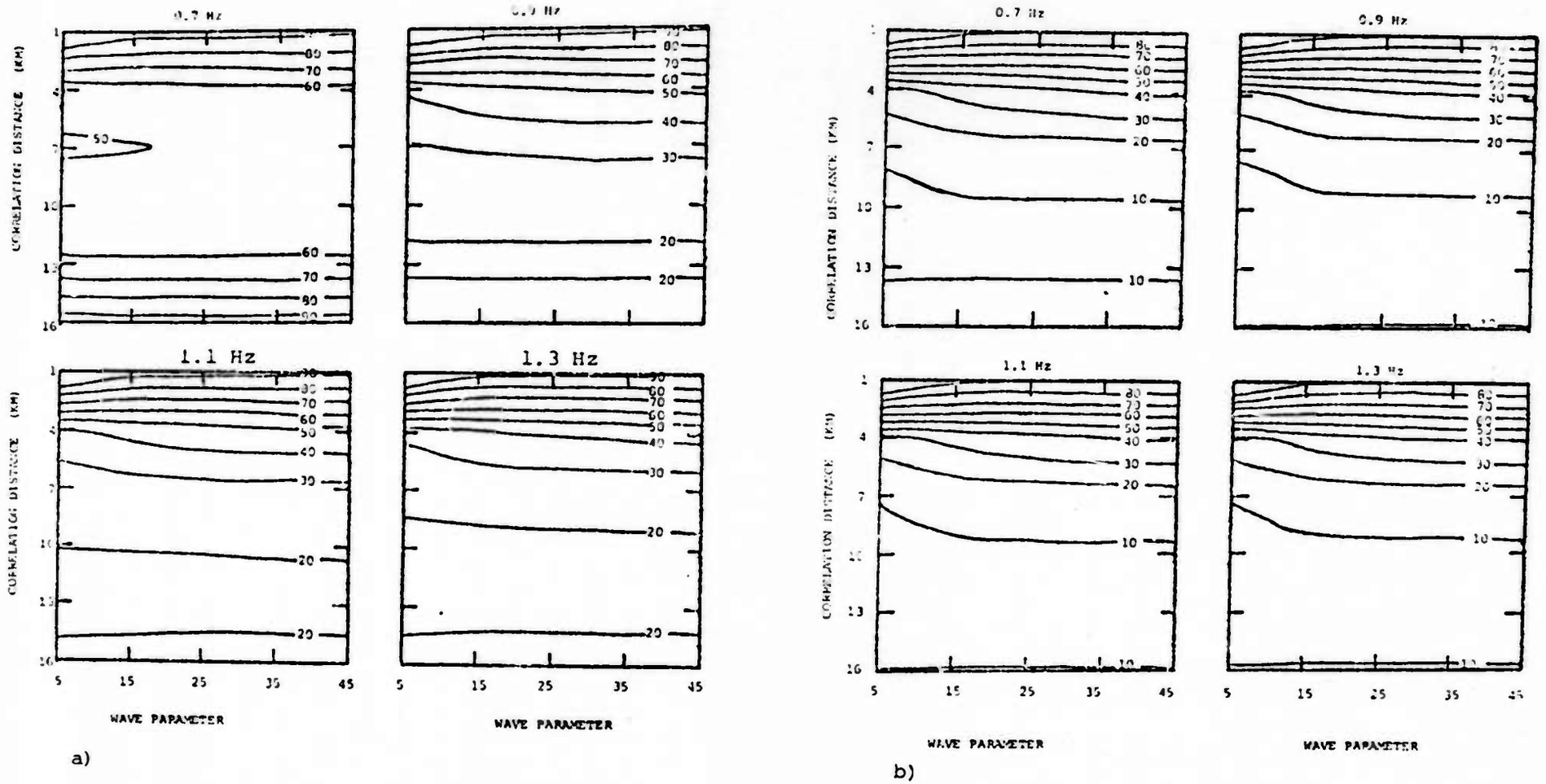

Fig. 5.2 Contour plots of per cent relative prediction error variance for travel time (a,b,c) and logamplitude (d,e,f) for different dominant frequencies (events from Table 1).

a) Event 2, time b) Event 4, time c) Event 6, time

d) Event 2, amp e) Event 4, amp f) Event 6, amp

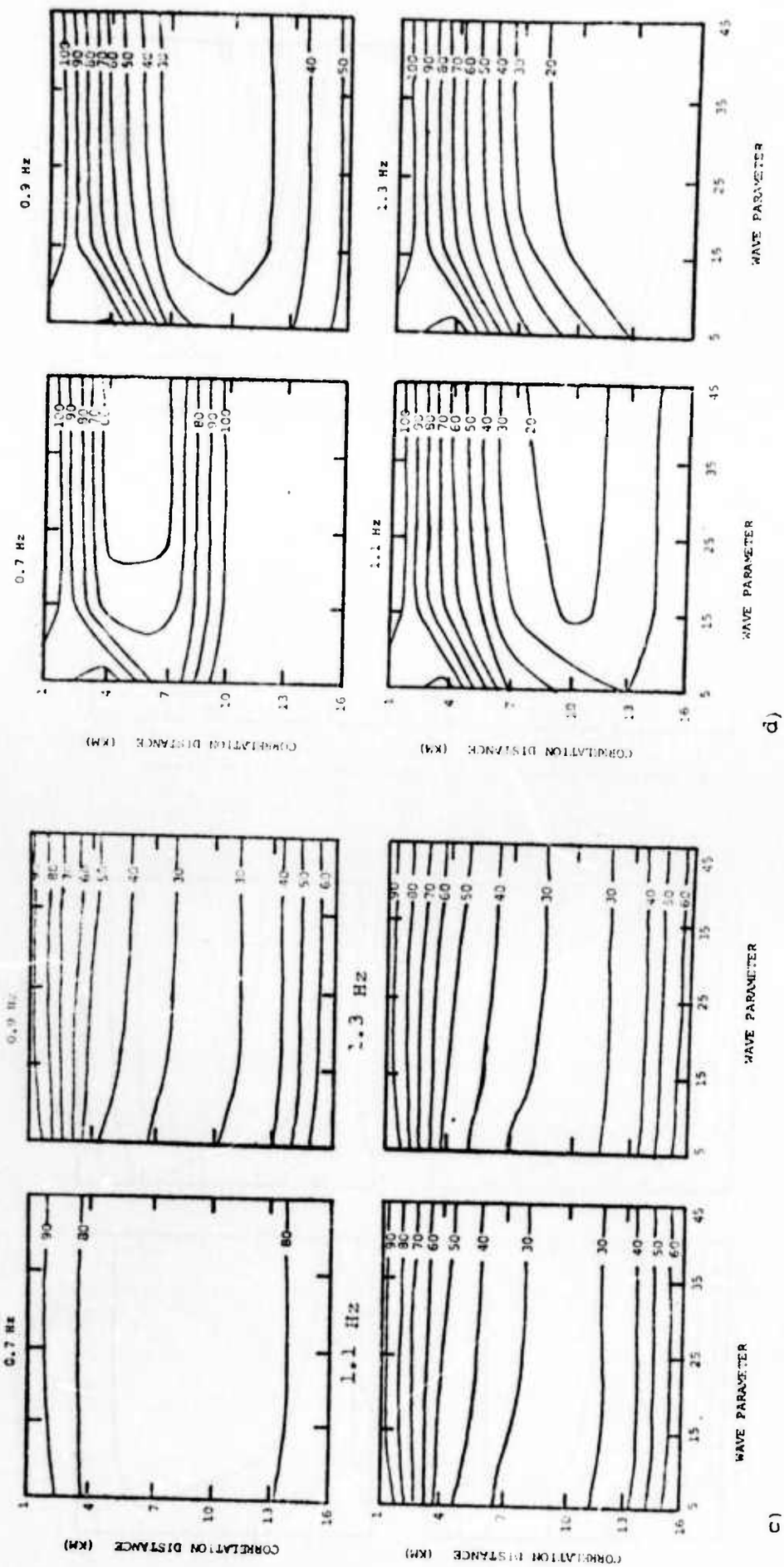
0.9 Hz
0.7 Hz
1.3 Hz
1.1 Hz
WAVE PARAMETER
CORRELATION DISTANCE (KM)
d)
c)

Fig. 5.2 (cont.)

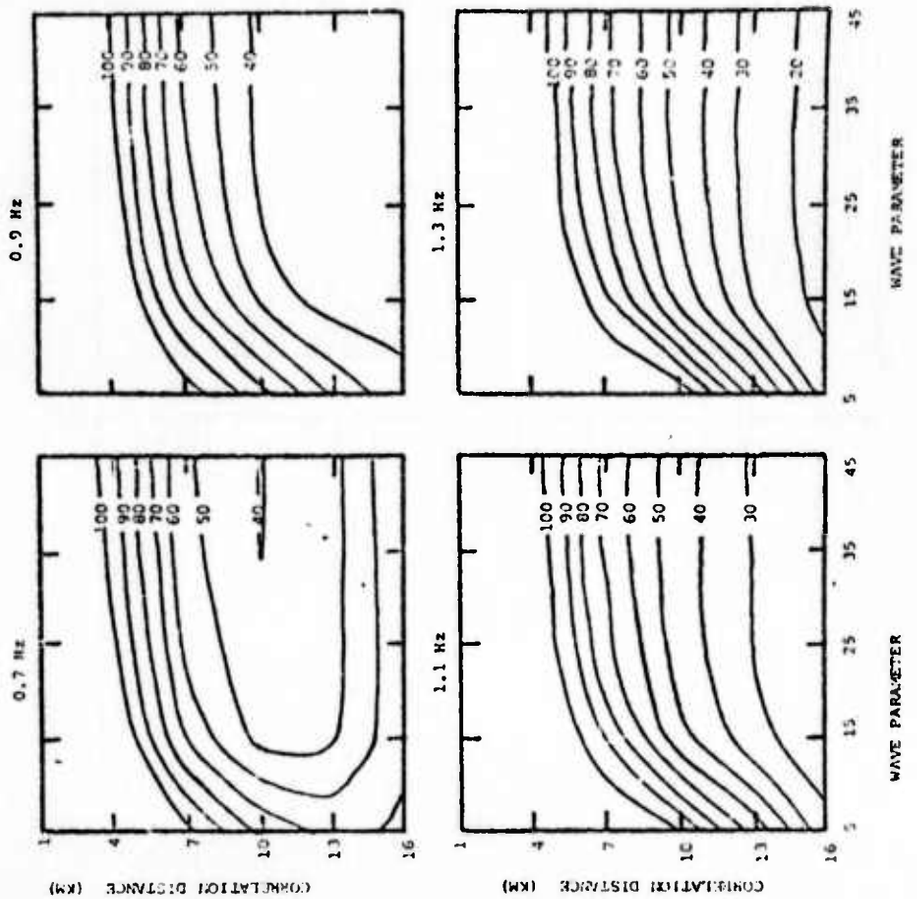

f)

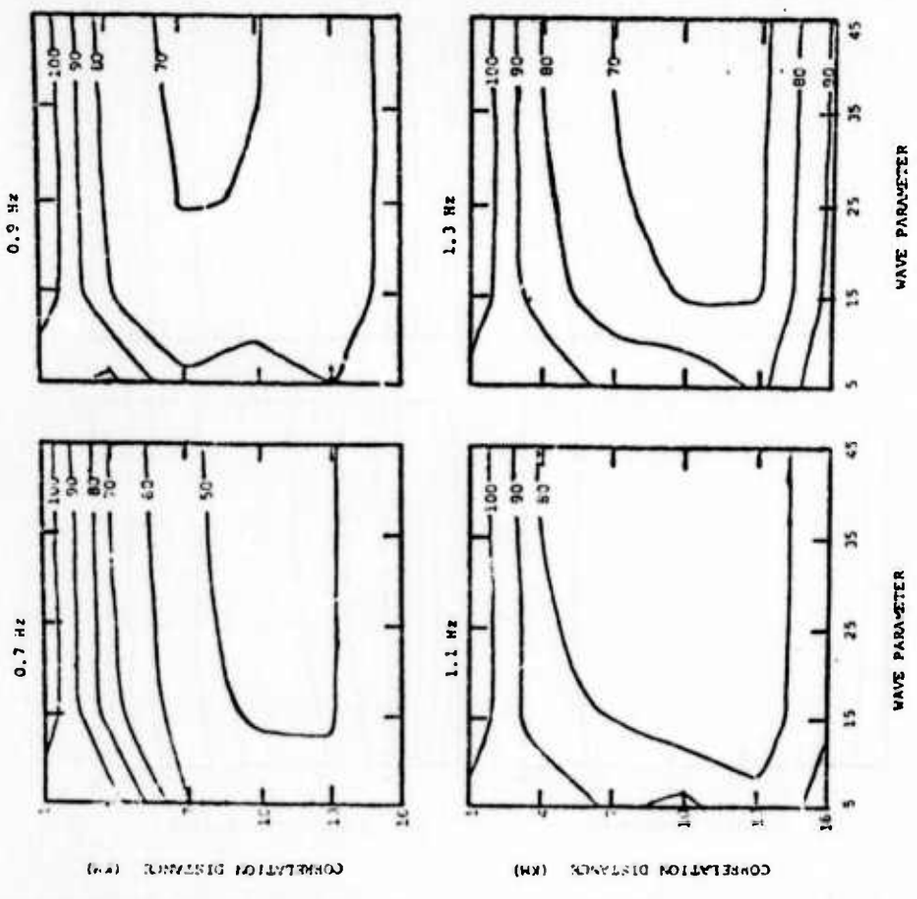

e)

Fig. 5.2 (cont.)

The minimum prediction error variance reflects the form of the symmetric correlation function best fitting the data. As seen from the contour plots of Fig. 5.2, there is no mimimum point in the range of (a,D) values examined. We observe, however, that there is a minimum trough running parallel to the D-axis, leaving this value undetermined but giving a quite well-defined correlation distance. Noteworthy, up to 90% of the plane wave residual variances can be explained as a stochastic "scattering" effect.

Fig. 5.3 shows the distribution of possible combinations versus horizontal station separation for the 54 instruments used in the prediction procedure. Since there is a definite minimum of information around 10 km, we could attribute the low correlation distance to a bias effect caused by nonuniformity in this distribution.

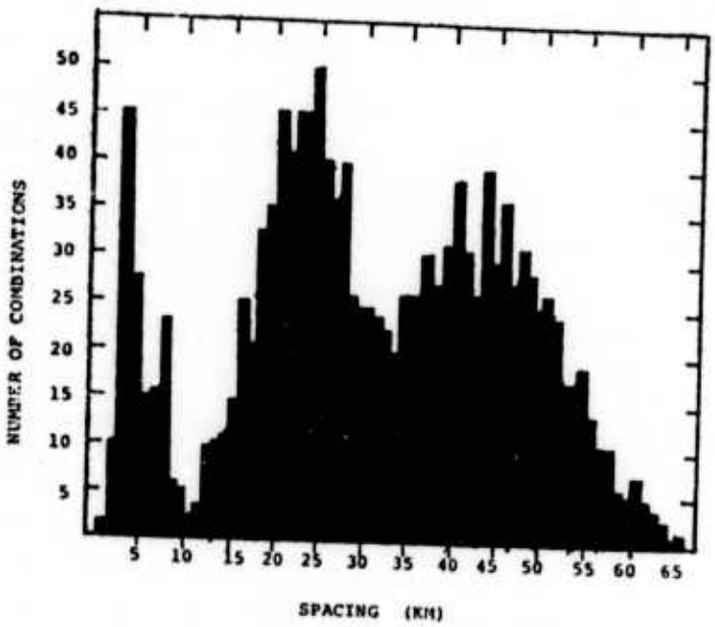

Fig. 5.3 Number of possible instrument combinations versus spacing for subarrays 01A, 01B,...,07B, 06C.

Among those correlation functions tried, which were of the type exponentials multiplied by polynomials, the Chernov type gave the best over-all performance. The empirical functions depicted in Fig. 4.4 were also smoothed and introduced in the prediction procedure, but with limited success. On the other hand, these functions should not be used unless all instruments were included in the prediction experiment since they are estimated for the whole array area.

5.2 Seismic Velocity - A Sample from Some Statistical Distribution

Measurement of a logarithmic amplitude should be associated with drawing a sample from a Gaussian distribution. This fact was mentioned already in the introduction, and is a valuable assertion made use of in analyzing seismic data (Ringdal, 1974). In view of seismic wave scattering, depending on what part of the wave front we consider across a network of stations like NORSAR, the wave-front normal points in different directions. Thus measuring velocity and azimuth (slowness) using stations with aperture of the order πa^2 (a is correlation distance), corresponds to estimation of a 'local' wave front normal and its associated velocity.

Mack (1972) introduces a wavenumber distribution to explain seismic signal coherency fall-off with sensor separation. His approach agrees well with the idea of non-planar wave fronts caused by small irregularities randomly distributed in the structure considered. The conventional velocity estimation technique applies to eq. (4.2.12) minimizing the residuals ϵ' assumed to be uncorrelated in space. In view of the previous sections, eq. (4.2.9) represents a far more realistic model for the teleseismic P travel times. The difference between the two methods is discussed in Dahle et al (1975) where it is pointed out that the choice between them is ruled by sensor separation and array aperture related to the correlation distance. In statistical terms, generalized least squares is a more 'effective' model when sensor separation is small and the array aperture not too large compared

to the correlation distance. Grouping the subarrays of NORSAR into seven subsets according to the scheme

Subset	Subarrays
I	01A,01B,07B
II	01C,02C,14C
III	02B,03C,04C
IV	03B,05C,06C
V	04B,07C,08C
VI	05B,09C,10C
VII	06B,11C,12C

provides the opportunity to obtain seven measurements of slowness for the same event. Slownesses were measured both using eq. (4.2.12), which we call Model I, and using eq. (4.2.9) denoted Model II. In the latter case a fixed correlation matrix was used, calculated from eq. (3.4.21a) with a=7 km and D=10. This correlation matrix was considered to

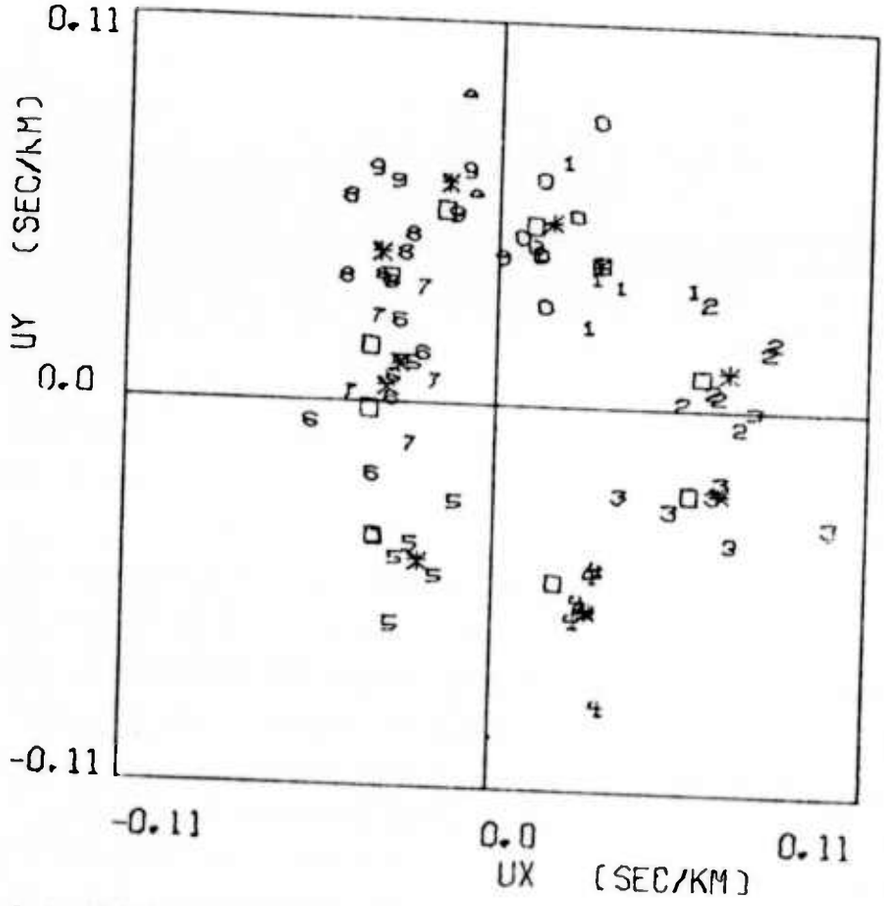

Fig. 5.4 Model I - Slowness estimates for subset I-VII for events 1-10 of Table 1. Symbol 0 corresponds to event 1, symbol 1 to event 2, etc. * indicates mean value of slowness for subset I-VII. □ indicates NOAA symmetrical earth solution.

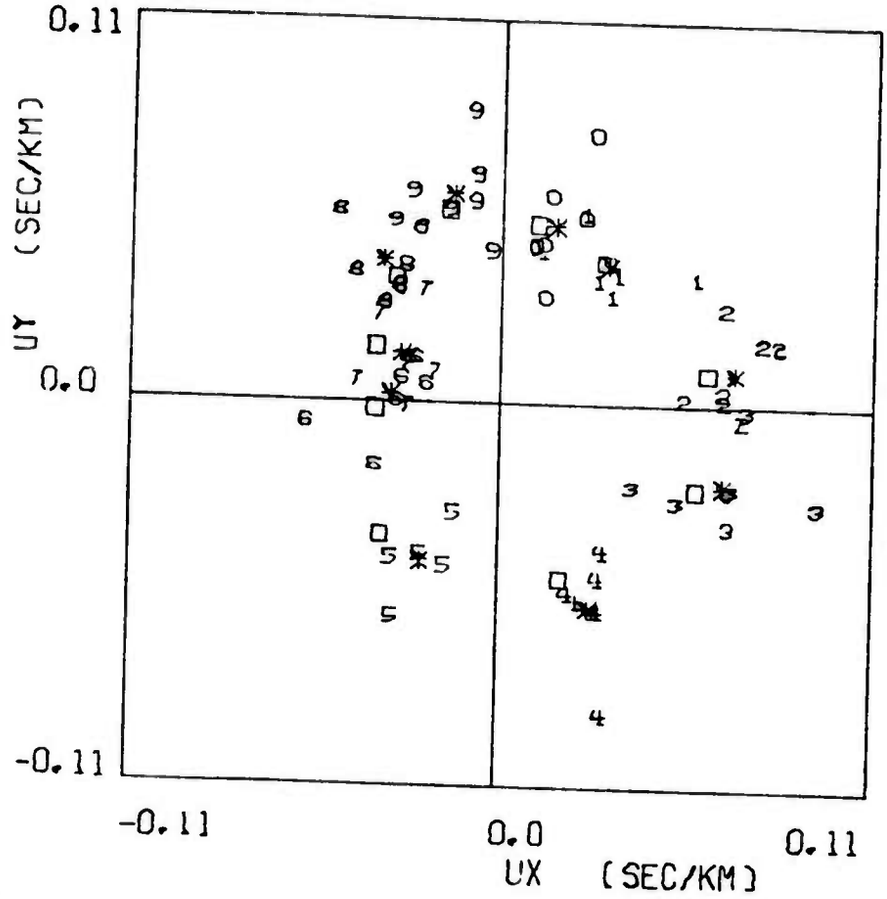

Fig. 5.5 Same as Fig. 5.4 for Model II.

be an optimum choice based on the prediction experiment results for the 0.7 Hz data of Fig. 5.2. The results obtained are shown in Fig. 5.4 for Model I and Fig. 5.5 for Model II. The effectiveness of the two methods was compared using the area of the 95% confidence ellipse calculated from the estimated slownesses (Dahle et al, 1975). The improvement of Model II relative to Model I is not easily seen by comparing Fig. 5.4 and 5.5 visually, but the numeric comparisons were conclusive . The U-space solutions presented in Figs. 5.4 and 5.5 reflect the complexity in the P-wave travel times across a seismic network like NORSAR, and show that application of small aperture seismic array measurements provides unreliable slowness estimates

so that a spatial sampling by a number of such arrays seems necessary in order to estimate an average wave front. The average slowness (stars) of Figs. 5.4 and 5.5 compared to the NOAA symmetrical earth solution (square) show the same picture as NORSAR's region correction vectors in Fig. 5.6, while individual estimates (numbers) provide the possibility of different interpretations.

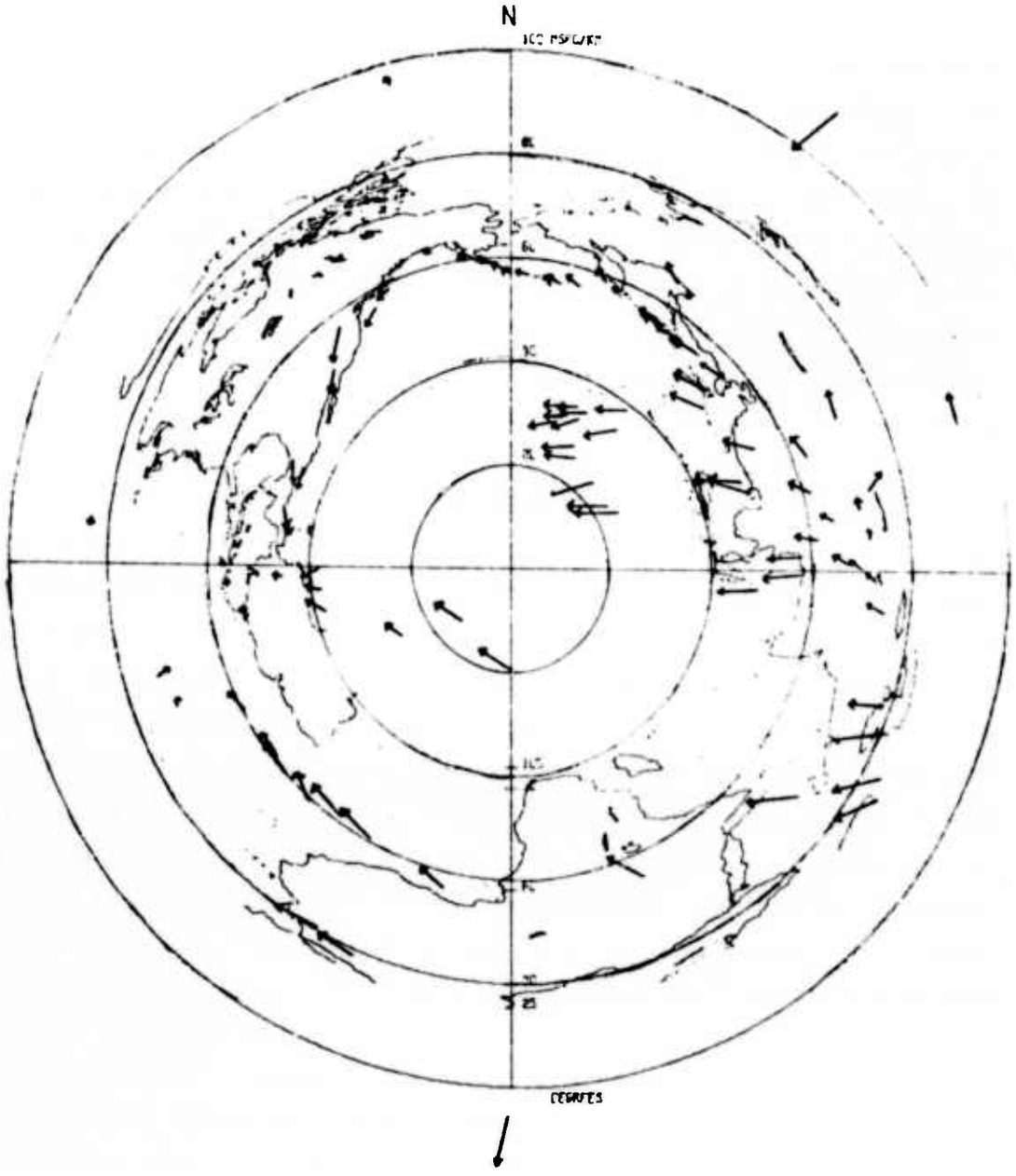

Fig. 5.6 Location calibration vectors plotted in slowness space. The tail of the arrow represents the observed point, while the head represents the NOAA solution.

6. CONCLUSIONS

The main purpose of this study has been to demonstrate the salient features of the fluctuations in seismological parameters as experienced at NORSAR, and to introduce an alternative to the homogeneous earth model. There is limited success with regard to the proposed scattering hypothesis; however, in our view the scattering approach deserves considerable attention. Such a conclusion is justified by the fact that the seismic wave field exhibits, to a satisfactory degree, some of the statistical qualities predicted by the theory. The assertion of forward scattering and mode conversion being basically P→P turns out to be an important point. As indicated in Section 4, there is reason to suspect the crust and upper mantle locally being inhomogeneous in a way not pertaining to Chernov's (1960) theory for weak inhomogeneities equally distributed throughout the medium. Stronger inhomogeneities giving rise to back-scattering, conversion to modes other than P and higher order scattering (scattered-scattered waves) are possible explanations of the discrepancies between theory and experience.

Substantial support to the scattering hypothesis is provided by the correlation functions depicted in Figs. 4.4 and 4.6. These are the features leading to the space predictive procedure outlined in Chapter 5, which also has been used in interpolation and extrapolation of point gravity measurements (Heiskanen and Moritz, 1967). The prediction procedure is important for two reasons. Firstly, because it shows the anomaly percentage explainable by correlated stochastic terms, and secondly, it provides a means of finding the optimum correlation matrix for the data (c.f. Fig. 5.2).

The realization of randomly corrugated seismic wave fronts is undoubtedly important in small aperture array seismology. We have, in our opinion successfully, related the fluctuations

in body wave travel time, local wave front normal and amplitude to wave scattering in an inhomogeneous crust and upper mantle. A quantitative description of the inhomogeneous medium is inconclusive for the moment, but our results show that attention must be paid to scattering effects when observed times or amplitudes are inverted into structural models.

Finally, as a comment to the large amplitude fluctuation across a seismic network like NORSAR, we see from Table 2 that the average standard deviation of logamplitudes is 0.4. This number gives rise to a standard deviation in magnitude measurements (assuming constant period) as forwarded by Veith and Clawson (1972) for a world wide network of stations reporting to USCGS.

ACKNOWLEDGEMENTS

The author is indebted to the entire NORSAR staff for their kind cooperation during the progress of this work. A special thanks is directed to Dr. Eystein Husebye for his guidance throughout the study. Valuable comments and discussions provided by Dr. H. Bungum and Mr. K.A. Berteussen during the preparation of the manuscript are greatly appreciated. Also the assistance of J. Fyen in computer-oriented problems and Mrs. L. Tronrud for typing the manuscript will be remembered. Finally, thanks to my colleague and room-mate cand. real. H. Gjøystdal for all his skilled support.

REFERENCES

Aki, K. (1973): Scattering of P-waves under the Montana LASA, J. Geophys. Res., 78.

Bendat, J.S., and A.G. Piersol (1966): Measurement and analysis of random data, J. Wiley and Sons, Inc.

Berteussen, K.A. (1974): NORSAR location calibrations and time delay corrections, NORSAR Scientific Report No. 2-73/74, NTNF/NORSAR, Kjeller, Norway.

Berteussen, K.A. (1975): Crustal structure and P-wave travel time anomalies at NORSAR, J. of Geophysics, 41, 71-84.

Berteussen, K.A., A. Christoffersson, E.S. Husebye and A. Dahle (1975): Wave scattering theory in analysis of P-wave anomalies at NORSAR and LASA, Geophys. J.R. Astr. Soc., 42, 403-417.

Bungum, H., and E.S. Husebye (1974): Analysis of the operational capabilities for detection and location of seismic events at NORSAR, Bull. Seism. Soc. Am., 64, No. 3, June.

Capon, J. (1974): Characterization of crust and upper mantle structures under LASA as a random medium, Bull. Seism. Soc. Am., 64.

Capon, J., and K.A. Berteussen (1974): A random medium analysis of crust and upper mantle structure under NORSAR, Geophys. Res. Lett., 1, 327-328.

Chernov, L.A. (1960): Wave propagation in a random medium, trans. by R.A. Silverman, McGraw-Hill Book Company, New York.

Christoffersson, A. (1975): Estimation of parameters characterizing a random medium, in Exploitation of Seismograph Networks (K.G. Beauchamp, ed.), Nordhoff-Leiden, The Netherlands, 463-470.

Cramér, H (1945): Mathematical methods of statistics, Uppsala.

Dahle, A., E.S. Husebye, K.A. Berteussen and A. Christoffersson (1975): Wave scattering effects and seismic velocity measurements, in Exploitation of Seismograph Networks, (K.G. Beauchamp, ed.), Nordhoff-Leiden, The Netherlands, 559-575.

Ferguson, T.S. (1967): Mathematical statistics, A decision theoretic approach, Academic Press, New York.

Gangi, A.F., and J.W. Fairborn (1968): Accurate determination of seismic array steering delays by an adaptive computer program, Supplemento al Nuovo Cimento, Serie 1, 6.

Gjøystdal, H. (1973): Methods of epicenter location using data from the two seismic arrays NORSAR and LASA, Cand. real. Thesis, University of Oslo, Norway.

Heiskanen, W.A., and H. Moritz (1967): Physical Geodesy, W.H. Freeman and Company.

Husebye, E.S., A. Dahle and K.A. Berteussen (1974): Bias analysis of NORSAR and ISC reported seismic event m_b magnitudes, J. Geophys. Res., 79, No. 20.

Jenkins, F.A., and H.F. White (1957): Fundamentals of optics, McGraw-Hill Book Company, Inc.

Johnston, J. (1963): Econometric methods, McGraw-Hill Book Company, New York.

Karal, F.C., and J.B. Keller (1964): Elastic, electromagnetic and other waves in a random medium, J. Mathm. Phys., 5, No. 4.

Knopoff, L., and J.A. Hudson (1964): Scattering of elastic waves by small inhomogeneities, J. Acoust. Soc. Am., 36.

Knopoff, L., and J.A. Hudson (1967): Frequency dependence of amplitudes of scattered elastic waves, J. Acoust. Soc. Am., 42.

Landers, T.E. (1971): Elastic waves in laterally inhomogeneous media, Ph.D. thesis, Stanford University, California, U.S.A.

Mack, H. (1972): Spatial coherence of surface waves, Seismic Data Analysis Center Report No. 8, Alexandria, Virginia.

Morrison, D.F. (1967): Multivariate statistical methods, McGraw-Hill Book Company, New York.

Morse, P.M., and H. Feshbach (1953): Methods of theoretical physics, McGraw-Hill Book Company, New York.

Ringdal, F. (1974): Estimation of seismic detection thresholds Technical report No. 2, Texas Instruments, Inc., Dallas, Texas.

Ringdal, F., E.S. Husebye and A. Dahle (1975): P-wave envelope representation in event detection using array data, in Exploitation of Seismograph Networks (K.G. Beauchamp, ed.), Nordhoff-Leiden, The Netherlands, 591-603.

Steinberg, B.D. (1965): Large aperture teleseismic array theory, ARPA report of first LASA Systems Evaluation Conference.

Tartarski, V.I. (1961): Wave propagation in a turbulent medium, trans. by R.A. Silverman, McGraw-Hill Book Company, New York.

Taylor, L.S. (1967): On Rytov's method, Radio Science, 2.

Veith, K.F., and G.E. Clawson (1972): Magnitude from short period P-wave data, Bull. Seism. Soc. Am., 63, No.2.